

Chapter 4

The intermediate-age open cluster Collinder 359

Young open clusters are ideal regions to place good constraints on the time spread of star formation for two reasons. First, cluster members less massive than about $0.8 M_{\odot}$ are displaced well above the ZAMS, making their identification easier. Second, low-mass stars and brown dwarfs remain bound to the cluster due to the limited dynamical evolution.

To identify complete and homogeneous samples of young very low-mass stars and brown dwarfs in clusters over large areas, a Canada-France-Hawaii Key Programme was initiated within the framework of our EC Research Training Network to survey about 80 square degrees in the I and z filters down to completeness limits of 22.0 in star-forming regions, open clusters and in the Hyades. One part of the project focused on five pre-main-sequence open clusters, including IC 4665, NGC 2232, Collinder 70, Stephenson 1, and Collinder 359. The analysis of the optical images yielded several hundreds bona-fide member candidates in each cluster down into the substellar regime, some of them being already followed-up in the near-infrared to weed out contaminating objects.

This chapter, devoted to the pre-main-sequence open cluster Collinder 359, is organised as follows. The CFHT Key Programme is presented in § 4.1 along with the target list and the main goals. A literature review of the present knowledge of Collinder 359 is given in § 4.2. The wide-field optical (I, z) observations of a 1.6 square degree area in Collinder 359 are detailed in § 4.3.1. The data reduction of the optical images is detailed § 4.3.2 and the extraction of the photometry described in § 4.3.3. The optical ($I, I-z$) colour-magnitude diagram is drawn § 4.3.4 and the cluster member candidates selection procedure described in § 4.3.5. The near-infrared follow-up of the optically-selected cluster member candidates in Collinder 359 is presented in § 4.4. The cluster luminosity and mass functions are derived in § 4.5 and § 4.6, respectively, including a discussion on the uncertainties on the age and distance of the cluster. Conclusions of the study of Collinder 359 and future projects are presented in § 4.7.

The data reduction and analysis of the CFH12K results from a large collaboration involving several teams within the European Network. The work described in this chapter has been mostly done by myself and will part of a forthcoming paper. I will continue to use “we” and not “I” to describe the results on Collinder 359 and to keep with the general principle of this thesis.

4.1 The CFHT Key Programme

4.1.1 Description of the CFHT Key Programme

A Canada-France-Hawaii Telescope (hereafter CFHT) Key Programme (30 nights over 2 years) centred on wide-field optical imaging of young, intermediate-age, and older open clusters (Bouvier, PI) was carried out within the framework of the European Research Training Network “The Formation and Evolution of Young Stellar Clusters” (McCaughrean, coordinator) to examine the sensitivity of the low-mass stellar and substellar IMF to time and environment.

The survey was conducted with a large-CCD mosaic camera (CFH12K) in the I and z filters down to detection and completeness limits of $I = 24.0$ and 22.0 , respectively, covering a total of 80 square degrees in a variety of environment, from star-forming regions (Serpens, Taurus, Ophiuchus, and Perseus), to pre-main-sequence open clusters (IC 4665, Collinder 359, Steph 1, Collinder 70, and NGC 2232), to the older Hyades. All regions are listed in Table 4.1 along with their coordinates (J2000), ages in Myr, distances in parsecs and diameters. The area surveyed in the optical with the CFH12K camera (and MegaCam when usable) are given in the last column of Table 4.1.

Table 4.1: List of star-forming regions (SFR), pre-main-sequence open clusters (PMS), and older clusters (OC) targeted within the framework of the CFHT Key Programme. Right ascension and declination (in J2000) are given in columns 3 and 4, respectively. Ages, distances, and diameters are listed in columns 5–7 (Open Star Cluster database and Lyngå 1987). The area surveyed in each cluster with the CFH12K camera is provided in the last column.

	Target	R.A.	Dec	Age	Distance	Diameter	Surv. Area
SFR	Perseus	03:35:00	+30:00:00	≤ 3 Myr	300 pc	—	6.5 deg ²
	Taurus	04:30:00	+20:00:00	≤ 3 Myr	140 pc	—	7.8 deg ²
	Ophiuchus	16:00:00	-25:00:00	≤ 3 Myr	145 pc	—	6.5 deg ²
	Serpens	18:30:00	+01:00:00	≤ 3 Myr	260 pc	—	5.9 deg ²
PMS	Collinder 70	05:33:00	-01:00:00	10 Myr	387 pc	140'	4.0 deg ²
	NGC 2232	06:24:00	-04:00:00	53 Myr	324 pc	45'	4.0 deg ²
	IC 4665	17:43:00	+05:00:00	43 Myr	352 pc	70'	4.2 deg ²
	Collinder 359	17:58:00	+02:00:00	32 Myr	249 pc	240'	1.6 deg ²
	Stephenson 1	18:51:00	+37:00:00	53 Myr	390 pc	20'	0.65 deg ²
OC	Hyades	04:24:00	+14:45:00	600 Myr	46 pc	12 deg.	17.3 deg ²

4.1.2 The choice of the optical filters

We have chosen to carry out the wide-field optical observations in the I and z filters mainly to optimise the search for low-mass stars and brown dwarfs in young clusters. This choice was also motivated by the results of 6.4 deg² imaging survey of the Pleiades with the CFH12K in the I - and z -bands (Moraux et al. 2003) conducted with the same telescope/instrument configuration. New brown dwarf candidates of the cluster were revealed and the cluster mass function, derived

from the previous study in the Pleiades by Bouvier et al. (1998), extended to $30 M_{Jup}$.

1. The sky background in (I,z) passbands is dominated by OH emission and not by the moon. The observations of Collinder 359 were carried out with a lunar phase of about 50 %.
2. The $I-J$ colours get redder towards low-mass cluster members, providing a good discriminant to separate the cluster sequence from field stars (Zapatero Osorio et al. 2000). Hence, we expect a similar behaviour for the $I-z$ colours.
3. The $I-z$ colours were found to be a good discriminant to weed out field stars from low-mass cluster members in the Pleiades (Cossburn et al. 1997; Zapatero Osorio et al. 1999; Moraux et al. 2003). We expect a similar trend, perhaps enhanced for younger pre-main-sequence objects than the Pleiades due to the redder colours.
4. Young brown dwarfs get redder in $R-I$ colours implying very faint R magnitudes which greatly hamper the detection of the least massive components of the cluster. Much longer exposure times in the R filter than in I are, therefore, required to compensate for this effect. To the contrary, we have achieved similar completeness and detection limits of 24.0 and 22.0, respectively, both in I - and z -bands with comparable exposure times of 300 sec and 360 sec in I and z .

4.1.3 Aims of the CFHT Key Programme

The main goals of CFHT Key Programme was to address the most pressing issues:

- How do brown dwarfs form and at which rate?
- What is the mass distribution of low-mass stars and brown dwarfs?
- Is there a lower mass limit to the Initial Mass Function?
- Is the Initial Mass Function sensitive to the environment?
- How do substellar objects evolve with time?

As a second step after membership assessment of the photometrically-selected cluster candidates, this large programme will aim at studying the evolution and properties of stellar and substellar objects in various environments:

- Test the evolutionary tracks using 10–50 Myr old open clusters.
- Age and mass dependence of the coronal and chromospheric activity of very low-mass stars.
- Mass dependence of the lithium depletion in very low-mass stars and brown dwarfs.
- Distribution of rotation rates as a function of mass.
- Distribution of rotational velocities of very low-mass stars as a function of age.
- Disk frequency and their lifetime.
- Distribution of wide binaries as a function of mass.

4.1.4 Selection of the pre-main-sequence open clusters

The selection of the five pre-main-sequence open clusters made use of the Open Cluster Database¹. The following criteria were applied to select the most suitable open clusters to answer the present issues within the framework of the CFHT Key Programme.

- Clusters with an age between 10 and 50 Myr
- Clusters less distant than 500 pc to be able probe the substellar regime
- Northern Hemisphere open clusters observable with the CFHT at Mauna Kea, Hawai'i
- A lower limit of 10° in galactic latitude to avoid significant contamination

Besides well-known open clusters such as the Pleiades, α Per, IC2391, IC2602, among others, five pre-main-sequence clusters satisfied the criteria listed above. The clusters were IC 4665, Stephenson 1, Collinder 70, NGC 2232, and Collinder 359, the latter constitutes the core of this chapter whose results will be published in a forthcoming paper. The main characteristics of the five selected open clusters are provided in Table 4.1, including coordinates, age, distances, and estimated diameters.

4.2 Literature on the open cluster Collinder 359

Collinder 359 (=Melotte 186) was selected as a 30 Myr open cluster at a distance of 250 pc, from a search in the Open Star Cluster webpage. The cluster is located in the Ophiuchus constellation around the star 67 Oph (Figure 4.1). The equatorial and galactic coordinates (J2000) of the cluster centre are: ($18^{\text{h}}01^{\text{m}}06\text{s}$, $+02^\circ 54'$) and ($29.7, +12.5$), respectively.

Collinder 359 was relatively unstudied and very little literature is available about the cluster. No deep optical survey had been carried out around the cluster centre, although several papers mention the cluster in passing. However, one needs to be polyglot to deal with papers in different languages such as French, English, and Russian! I will review the current knowledge on this cluster by summarising the content of major articles.

- Collinder 359 (=Melotte 186) was first seen on the Franklin-Adams Charts Plates and classified as a coarse cluster by Melotte (1915) within the framework of his large catalogue of globular and open clusters. It was described it as *a large scattered group of bright stars around 67 Ophiuchi (= HD164353), covering an area of about 6 square degrees.*
- In a large catalogue of open clusters, Collinder (1931) described Collinder 359 as *a group of about 15 stars with no appreciable concentration on the sky and no well-defined outline.* Cluster stars appear brighter than the surrounding stars but no bright stars stand out from the others. The diameter of the cluster was estimated to $240'$ and dimensions of $5^\circ \times 3^\circ$ were mentioned. The cluster contains thirteen stars listed in Table 4.2 and shown as filled hexagons in Figure 4.2. Collinder (1931) provided the coordinates, V magnitudes, spectral types for all 13 stars and additional proper motion information when available. Isochrone fitting to the five early-B stars yielded photometric parallax of 0.0048 ($d = 209$ pc) while the

¹<http://www.seds.org/messier/open.html>

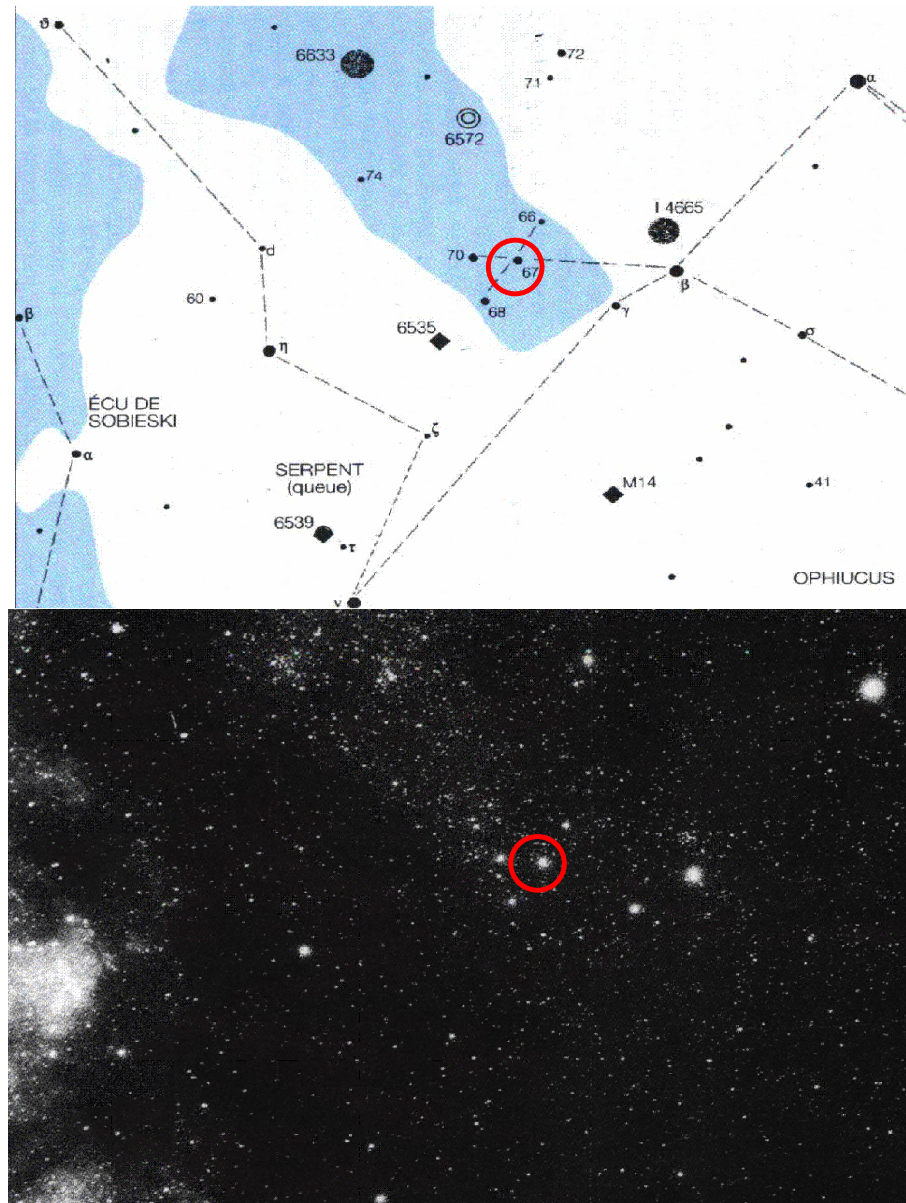


Figure 4.1: The upper panel is a schematic view of the location of the open cluster Collinder 359 (red circle) in the constellation of Ophiuchus, around the B5 supergiant, 67 Oph. The bright stars belonging to the constellation of Ophiuchus, Serpens and Scutum are marked with symbols representing their brightness. Other astronomical objects are indicated, including open clusters, globular clusters (diamonds), and planetary nebula (concentric circles). The lower panel is an image of the same region of the sky and at the same scale. *Courtesy: Astronomia.* For indication, the difference between α Oph and β Oph is about 2.1° and 8.0° in right ascension and declination, respectively. The difference between 67 Oph and 70 Oph is about 1.2° and $26'$ in right ascension and declination, respectively.

Table 4.2: This table lists the 13 bright stars within Collinder 359 as listed in Collinder (1931). Column 1 lists the running number of the member, column 2 gives the Henry Draper Catalogue number, columns 3 and 4 list the right ascension and the declination (in J2000), column 5 lists the spectral types Collinder (1931), columns 6, 7, and 8 lists the V magnitude and the $B-V$ and $U-B$ from Blanco et al. (1968), columns 9 and 10 list the $V-R$ and $R-I$, columns 11 and 12 list the proper motion of the object according to the SAO catalogue (1966). The membership of the object is given on the last column according to the discussion between Ruciński (1980) and Van't-Veer (1980).

	HD	RA	Dec	SpT	V	$B-V$	$U-B$	$V-R$	$R-I$	μ_α	μ_δ	M?
1	166233	18 09 33.8	03 59 35	F2	5.72	+0.37	+0.02	0.22	0.21	+0.0360	-0.007	NM
2	168797	18 21 28.4	05 26 08	B5	6.16	-0.02	-0.64	0.00	0.01	+0.0105	-0.004	NM
3	164353	17 58 08.3	02 55 57	B5 Ib	3.96	+0.04	-0.63	0.06	0.03	-0.0015	-0.010	M
4	164352	18 00 41.7	03 08 57	B8	9.33	-0.01	-0.39	0.02	0.06	-0.0015	-0.002	M
5	164284	18 00 15.8	04 22 07	B3	4.70	-0.04	-0.86	0.10	0.08	+0.0000	-0.013	NM
6	164283	17 57 42.4	05 32 37	A0	9.10	+0.26	+0.19	0.16	0.21	+0.0075	-0.014	M
7	164096	17 59 34.6	02 30 16	A2	9.70	+0.20	+0.17	0.13	0.20	-0.0105	-0.006	M
8	164097	17 59 29.5	02 20 37	A2	8.54	+0.17	+0.15	0.12	0.15	-0.0060	+0.003	M
9	164432	18 00 52.8	06 16 05	B3	6.35	-0.08	-0.77	-0.01	-0.01	+0.0015	-0.003	M
10	164577	18 01 45.2	01 18 18	A2	4.43	+0.04	+0.05	0.04	0.01	+0.0090	-0.012	NM
11	165174	18 04 37.3	01 55 08	B3	6.14	-0.01	-0.98	0.03	0.03	-0.0045	-0.003	NM
12	163346	17 55 37.5	02 04 29	A3	6.78	+0.56	+0.36	0.37	0.40	-0.0030	+0.007	NM
13	161868	17 47 53.5	02 42 26	A0	3.74	+0.03	+0.14	0.01	0.00	-0.0240	-0.074	NM

fainter B8–A2 stars gave a mean parallax of 0.0035 ($d = 286$ pc). However, the membership of these objects was not well established as neither proper motion nor photometric studies were available in Collinder 359. One object, 67 Ophiuchi, is a supergiant member of the cluster with a spectral type of B5Ib (Humphreys 1970).

- Searching in the 1958 *General Catalogue of Variable Stars* based on open clusters catalogued by Collinder (1931), Trumpler (1930), and others, Sahade & Frieboes (1960) extracted 10 W UMa-type stars within three cluster radii. A few years later, Sahade & Berón Dàvila (1963) concluded that none of the eclipsing binaries within the cluster were probable members. In a total of 26 eclipsing variables, 12 objects were classified as possible members while the remainder were unlikely to be members of Collinder 359.
- Blanco et al. (1968) compiled a huge photoelectric catalogue of more than 20,000 stars in the Galaxy in the UBV broad-band filters based on measurements extracted from the literature. The 13 stars mentioned by Collinder (1931) are included in this catalogue. The UBV magnitudes given in Table 4.2 are averaged values of all measurements available for those stars from the literature.
- The only age estimate of the cluster originates from the work by Wielen (1971) and Abt & Cardona (1983). The former derived an age ranging from 20 to 50 Myr with a mean value of 30 Myr using isochrone fitting based on three-colour photometry available in large catalogues of open clusters (Becker & Fenkart 1971). Abt & Cardona (1983) studied the distribution of Ap stars in open clusters as a function of age. A trend of older clusters having a larger number of Ap stars was noticed. Abt & Cardona (1983) put an upper limit of 30 Myr on the age of Collinder 359, assuming that 67 Oph is a member of the cluster, in agreement with the former determination.

- Akhundova (1971)² selected member candidates in Collinder 359 based on their proper motions. Using the magnitude versus spectral type relationship, and after rejection of likely non-members, Akhundova (1971) derived a distance of 350 pc and estimated the absorption to $A_V = 1.4$ mag.
- A discussion took place between Ruciński (1980) and Van't-Veer (1980) regarding the existence of W UMa-type systems in Collinder 359. While Ruciński (1980) noted that most of the stars listed by Collinder (1931) might actually be field stars, Van't-Veer (1980) argued the contrary based on homogeneous conversion of spectral types into colours. Van't-Veer (1980) found consistent distance moduli estimates from the B3 and A0 group of stars based on the $(M_V, B-V)$ colour-magnitude diagram. A few years later, Ruciński (1987) confirmed the results of Van't-Veer (1980) and concluded that stars n° 3, 4, 6, 7, 8, and 9 (Table 4.2) are bona-fide cluster members based on $BVRI$ CCD photometry. A distance modulus of 8.2 mag (distance = 436 pc) was derived from the isochrone fitting of the possible members.
- The 5th edition of the Open Cluster Data Catalogue (Lyngå 1987)³ provides a distance of 200 pc and a diameter of 240' for Collinder 359. The former is based on the estimate from the Bochum-Strasbourg magnetic tape catalogue of open clusters. The latter is taken from the work of Collinder (1931). However, no age was mentioned for Collinder 359.
- Baumgardt et al. (2000) confirmed cluster members in Collinder 359 from photometry, radial velocity and *Hipparcos* measurements. A mean proper motion of 0.42 ± 0.47 mas/yr in right ascension and -7.86 ± 0.35 mas/yr in declination was estimated. Parallax measurements yielded distances ranging from 317 to 460 pc, in agreement with isochrone fitting (Ruciński 1987). The parallax measurement from the supergiant 67 Oph led to a distance of 435^{+220}_{-110} pc (Perryman et al. 1997), consistent with the study by Baumgardt et al. (2000). Of the 13 possible members (Collinder 1931), only two share a common proper motion (stars n° 3 and 9; Table 4.2). Three other *Hipparcos* stars may be additional cluster members while the remaining objects were excluded as members.
- *Hipparcos* trigonometric parallaxes of five stars in Collinder 359 were used to derive photometric and spectroscopic distances, yielding estimates between 260 to 280 pc (Loktin & Beshenov 2001)⁴ with typical errors of about 20 pc.
- Combining the *Hipparcos* and Tycho 2 catalogues, a list of about 100 possible cluster members were extracted by Kharchenko et al. (2004, personal communication)⁵ based on their location within the cluster area and their proper motions. The position of these objects in the $(V, B-V)$ colour-magnitude diagram yielded a distance of 650 pc from isochrone fitting. The core and corona radii of the cluster were estimated to 0.4 and 1.1 degree, respectively.

To summarise, the current knowledge of Collinder 359 based on the available literature suggests an age of 30 Myr and a distance between 200 pc and 650 pc with a mean value of approximately 400 pc.

²This paper is in Russian and is not available at the ADS webpage

³The full catalogue can be accessed through the Centre de Données astronomiques de Strasbourg

⁴The data of the five stars were lost after the death of one of the author (A.V. Loktin, personal communication)

⁵Nina Kharchenko and Anatoly Piskunov visited our group at the AIP for a few months and kindly provided me with their results on Collinder 359 prior to submission

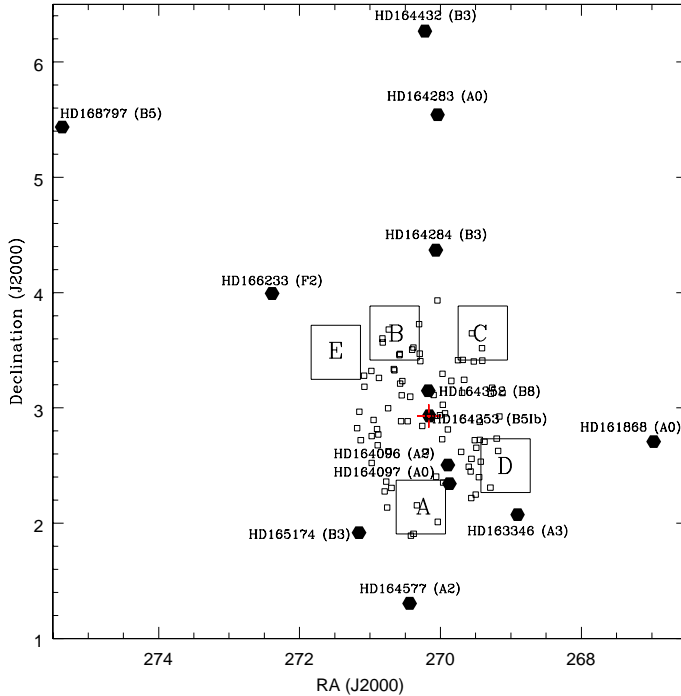


Figure 4.2: Location of the five CFH12K fields-of-view (A, B, C, D, and E) shown as boxes within the cluster area defined by the Open Cluster webpage. The 13 possible cluster members listed by Collinder (1931) are displayed as filled hexagons (Table 4.2). Their names and spectral types are provided as well. The open squares are the possible cluster members used for isochrone fitting by Kharchenko et al. (2004; personal communication), yielding a distance of 650 pc.

4.3 The wide-field optical survey of Collinder 359

We initiated a wide-field optical survey in the I and z filters down to a detection limit of 24.0 to study the very low-mass stars and brown dwarfs in the pre-main-sequence open cluster, Collinder 359.

4.3.1 The CFH12K wide-field optical observations

Five CFH12K frames were obtained on 18 and 20 June 2002 in Collinder 359 in the I and z filters, covering a total area of 1.6 square degrees in the cluster (Table 4.3). Figure 4.2 displays the location of the five CFH12K fields-of-view within the cluster area. Thirteen possible members as listed by Collinder (1931) (filled hexagons) are included as well. The CFH12K frames were chosen to avoid bright cluster members.

Fields A, B, C, and D were obtained on 18 June 2002 under photometric conditions with seeing ~ 0.8 arcsec. The remainder field, field E, was observed on 20 June 2002 under non-photometric conditions. The coordinates of the five CFH12K fields-of-view are provided in Table 4.3 along with the journal of the observations. Three sets of exposures were taken for each field-of-view:

short, medium, and long exposures with integration times of 2, 30, and about 900 seconds, respectively. The long exposures were exposed three times 300 and 360 seconds in the I and z filter, respectively, yielding detection limits of 24.0 in both passbands. Only one image was taken for the short and medium exposures, whereas three dithered positions were obtained for the long exposures, allowing rejection of bad pixels and removal of bad columns. The observations were scheduled in a queue mode so that the short, medium, and long exposures in the I -band were taken first, immediately followed by the short, medium, and long exposures in the z -band.

The CFH12K is a CCD mosaic camera dedicated to high-resolution wide-field imaging⁶. The camera comprises 12 chips of 4128×2080 pixels with a pixel scale of $0.206''$, yielding a field-of-view of $42' \times 28'$. Hence, no problem of undersampling was foreseen even during excellent conditions on Mauna Kea, which was the case for our observations. The cosmetic of the CFH12K mosaic was excellent with a total of 200 bad columns, most of them were concentrated on CCD05. The CCD06, CCD08, CCD09, CCD10, and CCD11 are entirely free of bad columns. The read-out time of the 12 chips was small (58 seconds). The camera has an excellent response in the red part of the spectrum as well, better than MegaCam, partly compensating for the smaller field-of-view.

Table 4.3: Coordinates of the five CFH12K fields-of-view along with the journal of observations obtained in the pre-main-sequence open cluster Collinder 359. The times of observations are given in UT and correspond to the beginning of the short exposures in the I -band.

Field	R.A. (J2000)	Dec (J2000)	Obs. Date	Time of obs. (UT)
A	18:01:06.60	+02:07:26.0	2002–06–18	08h19m15s
B	18:02:36.90	+03:37:52.7	2002–06–18	09h07m43s
C	17:57:36.90	+03:37:56.1	2002–06–18	09h56m07s
D	17:56:16.40	+02:29:46.4	2002–06–18	11h52m24s
E	18:05:55.70	+03:28:58.4	2002–06–20	12h29m20s

4.3.2 The data reduction of the wide-field optical images

The initial data reduction was provided by the Elixir pipeline and was mostly executed by David James at the CFHT Headquarters. Elixir is not a single program or package but a collection of programs, databases, and other tools related to the processing and evaluation of data obtained at the telescope. This pipeline includes bias subtraction, flat-fielding, correction for scattered light in the I and z bands, combining the dithered frames in case of long exposures, and astrometric solution provided in the header of the fits files. Standard stars were observed throughout the nights and were monitored constantly by the Elixir/Skyprobe tool to provide accurate zero-points.

The data reduction procedure to extract a catalogue of all objects from the reduced and stacked images processed by the pipeline was identical for each CFH12K field-of-view. The procedure presented in this paragraph is the result of intense discussions and close collaboration between the Grenoble, Potsdam, and Arcetri (EC network) teams to achieve a common and consistent data reduction for the wide-field optical images of the pre-main-sequence open clusters obtained within

⁶The camera is now superseded by MegaCam on the CFH 3.6-m telescope

the framework of the CFHT Key Programme. The major steps of the data reduction procedure are described below:

1. **Find the offsets between the I - and z - band images.** The telescope should theoretically point at the same position on the sky both in I - and z -bands as the coordinates provided by the user are identical for both filters. However, we have found shifts of order few pixels (2 to 5 pixels typically) between the I and z images. Three random stars were generally enough to correct for the differences in (x,y) coordinates between the I and z images. The task *imexamine* in IRAF was used to find the shifts. Tables 4.4, 4.5 and 4.6 provide the shifts (in integer pixels) of the z image relative to the I image. The CCD09 sometimes exhibits shifts larger than typically observed and affected fields A and C in the case of Collinder 359. The cause of this discrepancy is under investigation.
2. **Trim the I - and z - band images at [1:2048,1:4096].** Although not mandatory, the overscan regions in each chip in the I and z images were removed to avoid subsequent problem while running the extraction of the photometry with SExtractor. Indeed, some bright lines and columns affected the edges of the raw images, yielding overflow problems during the extraction of the photometry. Trimming was applied to both I and z images using the task *imcopy* in IRAF.
3. **Combine the I - and z - band images.** This step brings two advantages. First, the signal-to-noise ratio is increased by a factor of $\sqrt{2}$, allowing detection of fainter sources close to the detection limit ($I \sim z \sim 24.0$). Second, SExtractor has the ability to run the source detection on one image and extract the photometry on another image. Hence, the coordinates given in the final catalogues result from the combined (I,z) images whereas the photometry is extracted from the individual trimmed and shifted images. The astrometry of the faintest sources is thus more accurate than the astrometry from a single passband measurement.
4. **Run SExtractor and PSFEx.** Both packages were ran on each individual CCD of each CFH12K field-of-view for the short, medium, and long exposures in the I and z filters, respectively. A total of 180 (5 Fields \times 12 chips \times 3 exposures) catalogues were generated and contain coordinates (J2000), I and z magnitudes for each source, as well as other source parameters, including the ellipticity, FWHM, and quality of the photometry. A description of the parameters gathered in the final catalogues is given in the next section (§ 4.3.3).
5. **Apply zero points for photometric calibration.** To calibrate the photometry, the I and z magnitudes were corrected for the zero points listed on the Elixir webpage⁷. The CFH12K nominal zero points for the I - and z - bands are:

$$\begin{aligned} ZP(I) &= 26.184 \pm 0.023 \\ ZP(z) &= 25.329 \pm 0.031 \end{aligned}$$

These zero point values originates from the best quality set of standard stars observed with the CFH12K camera and collected over several years. However, we have applied a slight correction to the zero points to take into account the conditions of the night of the observations⁸. The corrections to the I and z filters were -0.0055 and +0.0575 for the first night

⁷<http://www.cfht.hawaii.edu/Instruments/Elixir/stds.2003.06.html>

⁸<http://www.cfht.hawaii.edu/cgi-bin/uncgi/elixir/skyprobe.pl?2002.06>

Table 4.4: Offsets (in integer pixels) between the I and z short exposure images.

CCD	Field A	Field B	Field C	Field D	Field E
00	(+5,+1)	(+4,+2)	(+4,+2)	(+3,+2)	(+3,-1)
01	(+4,+0)	(+3,+2)	(+4,+2)	(+3,+3)	(+2,-1)
02	(-2,+0)	(-3,+2)	(-4,+2)	(-3,+3)	(-2,-1)
03	(-3,+1)	(-2,+2)	(-2,+2)	(-3,+3)	(-1,-1)
04	(+1,+1)	(+2,+3)	(+1,+2)	(+2,+4)	(+0,+0)
05	(+1,+1)	(+2,+2)	(+1,+2)	(+1,+4)	(+0,-1)
06	(+4,-1)	(+4,+0)	(+4,+0)	(+4,-2)	(+3,+2)
07	(+4,+0)	(+3,-1)	(+4,+0)	(+4,-2)	(+3,+2)
08	(+3,+0)	(+3,-1)	(+3,-1)	(+3,-3)	(+2,+2)
09	(+2,+0)	(+2,-1)	(+2,-1)	(+2,-3)	(+1,+2)
10	(+0,+0)	(+1,-1)	(+1,-1)	(+1,-3)	(+1,+2)
11	(+1,-1)	(+1,-1)	(+1,-1)	(+1,-3)	(+0,+2)

Table 4.5: Offsets (in integer pixels) between the I and z medium exposure images.

CCD	Field A	Field B	Field C	Field D	Field E
00	(+5,+4)	(+4,+0)	(+4,+1)	(+4,+1)	(+3,+1)
01	(+4,+4)	(+3,+1)	(+4,+2)	(+4,+1)	(+3,+1)
02	(-3,+4)	(-3,+1)	(-3,+2)	(-3,+1)	(-2,+1)
03	(-3,+4)	(-2,+1)	(-3,+2)	(-3,+1)	(-2,+1)
04	(+2,+4)	(+1,+1)	(+1,+2)	(+2,+2)	(+1,+1)
05	(+2,+4)	(+1,+1)	(+1,+2)	(+2,+1)	(+1,+1)
06	(+4,-3)	(+4,+1)	(+4,+0)	(+4,+0)	(+3,+0)
07	(+4,-3)	(+3,+1)	(+4,-1)	(+4,+0)	(+3,+0)
08	(+3,-3)	(+2,+1)	(+3,-1)	(+3,-1)	(+2,+0)
09	(+2,-3)	(+2,+0)	(+2,-1)	(+3,-1)	(+2,+0)
10	(+2,-3)	(+1,+0)	(+1,-1)	(+2,-1)	(+1,+0)
11	(+1,-4)	(+1,+0)	(+2,-2)	(+2,-1)	(+1,+0)

Table 4.6: Offsets (in integer pixels) between the I and z long exposure images.

CCD	Field A	Field B	Field C	Field D	Field E
00	(+4,+1)	(+4,+1)	(+4,+1)	(+4,+0)	(+3,+0)
01	(+4,+2)	(+4,+1)	(+3,+1)	(+3,+0)	(+3,+0)
02	(-3,+2)	(-3,+1)	(-3,+1)	(-3,+0)	(-2,+0)
03	(-2,+2)	(-2,+2)	(-2,+2)	(-2,+0)	(-2,+0)
04	(+1,+2)	(+1,+2)	(+1,+1)	(+2,+1)	(+1,+0)
05	(+1,+2)	(+1,+2)	(+1,+1)	(+1,+1)	(+1,+0)
06	(+4,-1)	(+4,+0)	(+3,+0)	(+3,+1)	(+3,+0)
07	(+3,-1)	(+4,+0)	(+3,+0)	(+3,+0)	(+3,+1)
08	(+2,-1)	(+3,-1)	(+3,+0)	(+3,+0)	(+2,+0)
09	(+30,+29)	(+2,-1)	(-27,-30)	(+2,+0)	(+2,+0)
10	(+2,-1)	(+2,-1)	(+1,+0)	(+1,+0)	(+3,+1)
11	(+1,-2)	(+1,-2)	(+1,-1)	(+1,+0)	(+3,+0)

(18 June 2003) and -0.013 and +0.011 for the second night (20 June 2002), respectively. Those corrections to the zero points were computed from two standard stars bracketing the observations of fields A, B, C, and D on the 18 June 2002 whereas only one standard star was observed before the observations of field E. The Elixir/Skyprobe software indicated that the first night (18 June 2003) was photometric until 10h30 (UT) so that fields A, B, and C were observed under photometric conditions and good seeing conditions. However, the rest of the night was non-photometric with attenuation up to 0.1 mag, affecting the observations of field D. The Elixir/Skyprobe software indicated small variations of order of 0.050 mag during the observations of field E, taken on the second night (20 June 2002).

4.3.3 The extraction of the photometry

We have used the SExtractor software⁹ (Bertin & Arnouts 1996) to extract the photometry from the wide-field optical survey carried out with the CFH12K camera. However, although very efficient to distinguish stars from extended sources, SExtractor is only capable of aperture photometry. We have been kindly provided by the PSFEx package¹⁰ specially developed to extract PSF fitting photometry. We have favoured the PSF fitting to the aperture photometry because it provided more accurate photometric measurements for faint sources, which are, in our case, the cluster brown dwarf candidates.

The extraction of the photometry using the SExtractor and PSFEx packages was a three-step procedure. First, relatively bright stars (but not saturated!) were extracted with a reasonable detection threshold above the sky background. Next, a number of isolated objects suitable for point-spread function modelling were selected. A point-spread function was created for each individual chip and each exposure with the selected stars. However, one main drawback of the PSF modelling is the impossibility for the user to check interactively the reliability of the selected stars for the PSF computation. From our experience, the results were satisfactory though. Finally, SExtractor was run a second time, with the PSF created in the previous step, to detect all sources in the field-of-view and extract the photometry. The last step allowed us to cross-correlate the I and z catalogues through the *assoc_name* parameter keyword. The matching was done in pixel coordinates and not in celestial coordinates. The accuracy was better since the I and z images were previously shifted to the same pixel coordinate system.

To illustrate the procedure described above, the example of a script to run the SExtractor and PSFEx packages is given below.

1. **sex** imaI.fits -c default.sex -catalog_name psfI.cat -checkimage_name backgI.fits
2. **psfex** psfI.cat coll359I.psfex -checkimage_name psfI.fits
3. **sex** combIZ.fits,imaI.fits coll359I.sex -catalog_name catI.cat -checkimage_name resI.fits
4. **sex** imaZ.fits -c default.sex -catalog_name psfZ.cat -checkimage_name backgZ.fits
5. **psfex** psfZ.cat coll359Z.psfex -checkimage_name psfZ.fits

⁹<http://astroa.physics.metu.edu.tr/MANUALS/sextaror/>

¹⁰The PSFEx package is not freely available as the SExtractor package

```
6. sex combIZ.fits,imaZ.fits coll359Z.sex -catalog_name catIZ.cat -checkimage_name resZ.fits  
-assoc_name catI.cat
```

The input are the trimmed I , z , and combined (I, z) images referenced as imaI.fits, imaZ.fits, and combIZ.fits, respectively. The sex and psfex keywords written in bold letters correspond to the executables of the SExtractor and PSFEx packages, respectively. The words written in italics are the parameter keywords listed in the default.sex configuration file. We choose to assign the file names to the keywords *catalog_name* and *checkimage_name* on the command line to create a single configuration file template for all chips. However, these parameters can also be modified directly in the default.sex file.

The default.sex configuration file contains the main detection (threshold, deblending) and photometric (aperture size, zero points) parameters as well as header keywords, including the gain, and pixel size. The coll359I.sex and coll359Z.sex are copies of the default.sex configuration file for the I and z filters, respectively.

The output files from the whole procedure are the PSF, background, and residual images denoted as psfI.fits (psfZ.fits), backgI.fits (backgZ.fits), and resI.fits (resZ.fits) for the I (z) filters. The psfI.cat and psfZ.cat files are binary files containing the stars selected for the PSF modelling. The psfI.fits and psfZ.fits images represent the PSF of one chip of one CFH12K field-of-view. The background images correspond to the variation of the sky background across the whole chip. We adjusted the parameters in the default.sex configuration file with cautiousness to take into account the background variation around bright stars. The residual images represent the science frame after removal of all sources by the PSF taken from the psfI.fits and psfZ.fits files. Figure 4.3 shows the science frame corresponding to one CCD chip of one CFH12K field-of-view, as well as the corresponding PSF, background and residual images.

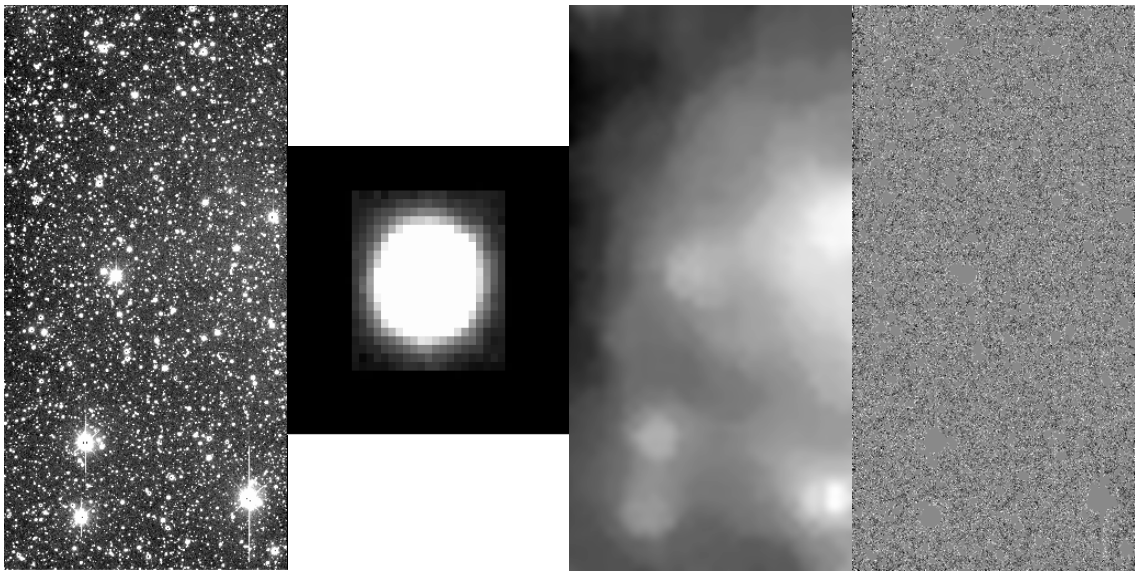


Figure 4.3: Output images from the extraction of the photometry using SExtractor and PSFEx. From left to right are shown the science frame corresponding to one CCD chip of one CFH12K field-of-view, the corresponding PSF, background and residual images after object subtraction.

The six steps described above were repeated for each CCD chip of the CFH12K in each field-of-view (A, B, C, D, and E) for all three exposures (short, medium, and long), generating a total of 180 catalogues. The final output catalogues contain the following parameters (bold font and capital letters) which we have selected to be of interest for our purposes:

- **ID** is the number of the object.
- **FLUX_PSF** is the flux contained within the PSF in counts.
- **FLUXERR_PSF** is the error on the flux contained within the PSF in counts.
- **MAG_PSF** is the magnitude derived from the psf fitting in mag.
- **MAGERR_PSF** is the error on the magnitude derived from PSF photometry. Up to now, no error estimate is provided.
- **MAG_APER** is the magnitude derived from aperture photometry (in mag).
- **MAGERR_APER** is the rms error vector on the magnitude derived from aperture photometry (in mag).
- **X_IMAGE** is the X position of the object.
- **Y_IMAGE** is the Y position of the object.
- **ALPHA_J2000** is the right ascension of the object in degrees (in J2000).
- **DELTA_J2000** is the declination of the object in degrees (in J2000).
- **ELONGATION** is the ratio of the profile rms along the ellipse axis.
- **ELLIPTICITY** is equal to (1–ELONGATION).
- **FWHM_IMAGE** is the full-width-half-maximum of the object or seeing if we take into account the pixel scale of the CFH12K camera ($0.206''/\text{pix}$). Values lower than 1 indicate bad pixels while large values correspond to extended sources. We have considered objects spanning 1–5 in FWHM for the subsequent analysis.
- **FLUX_RADIUS** is the flux contained in half of the FWHM.
- **FLAGS** are internal flags evaluating the quality of the photometry. They are multiple of 2 ranging from 0 to 64. A flag of 0 indicate good photometry. We have considered only objects with flag values lower than four.
- **VECTOR_ASSOC** is the associated parameter vector which adds two columns, namely the PSF magnitude in the *I*-band and its associated error.

Before discussing the colour-magnitude diagram and the selection of cluster member candidates, a number of “checks” were required to insure the validity of the output catalogues in terms of colour and photometry. If the photometric calibrations were perfect, all colour-magnitude diagrams of each individual chip and field-of-view of the CFH12K camera should be aligned on top of each other. However, we found colour shifts between individual chip, between fields-of-view, and between the short, medium, and long exposures for all three pre-main-sequence open clusters (IC4665, Steph 1, and Collinder 359) and for the Serpens observations. We have no explanation for the cause of these colour shifts. Note that we have corrected for the z -band scattered light. We describe below the procedure applied to correct for those colour shifts.

Table 4.7: Colour shifts between individual chip for each CFH12K field-of-view for the short exposures. The reference is the CCD 04. Negative and positive values indicate blue and red colour shifts of the colour-magnitude diagram, respectively.

CCD	Field A	Field B	Field C	Field D	Field E
00	-0.057	-0.035	-0.062	-0.057	-0.014
01	-0.055	-0.075	-0.061	-0.083	-0.024
02	-0.051	-0.075	-0.070	-0.076	-0.051
03	-0.054	-0.070	-0.037	-0.042	-0.028
04	+0.000	+0.000	+0.000	+0.000	+0.000
05	-0.010	+0.004	-0.017	+0.030	+0.012
06	-0.072	+0.030	+0.010	+0.004	+0.027
07	-0.103	-0.070	-0.023	-0.042	-0.019
08	-0.181	-0.110	-0.103	-0.094	-0.090
09	-0.137	-0.128	-0.129	-0.120	-0.081
10	-0.103	-0.122	-0.072	-0.061	-0.034
11	-0.077	-0.070	-0.057	-0.047	-0.040

Table 4.8: Colour shifts between individual chip for each CFH12K field-of-view for the medium exposures. The reference is the CCD 04. Negative and positive values indicate blue and red colour shifts of the colour-magnitude diagram, respectively.

CCD	Field A	Field B	Field C	Field D	Field E
00	-0.014	+0.023	-0.011	-0.002	-0.007
01	-0.026	-0.032	-0.049	-0.036	-0.029
02	-0.061	-0.044	-0.082	-0.039	-0.042
03	-0.013	-0.018	-0.012	-0.022	-0.014
04	+0.000	+0.000	+0.000	+0.000	+0.000
05	+0.040	+0.039	+0.038	+0.030	+0.022
06	+0.018	+0.023	+0.003	+0.023	+0.012
07	-0.051	-0.021	-0.020	-0.018	-0.016
08	-0.081	-0.070	-0.059	-0.074	-0.054
09	-0.090	-0.112	-0.090	-0.110	-0.086
10	-0.026	-0.035	-0.027	-0.035	-0.028
11	-0.021	-0.058	-0.027	-0.021	-0.024

Table 4.9: Colour shifts between individual chip for each CFH12K field-of-view for the long exposures. The reference is the CCD 04. Negative and positive values indicate blue and red colour shifts of the colour-magnitude diagram, respectively.

CCD	Field A	Field B	Field C	Field D	Field E
00	-0.006	+0.020	+0.000	+0.028	+0.023
01	-0.028	-0.025	-0.029	+0.002	+0.004
02	-0.050	-0.036	-0.055	-0.065	-0.021
03	-0.025	-0.030	-0.038	-0.035	+0.001
04	+0.000	+0.000	+0.000	+0.000	+0.000
05	+0.050	+0.038	+0.063	+0.030	+0.045
06	+0.006	-0.006	+0.036	+0.016	+0.063
07	-0.038	-0.019	-0.017	-0.006	+0.005
08	-0.069	-0.062	-0.064	-0.075	-0.041
09	-0.097	-0.076	-0.077	-0.092	-0.066
10	-0.023	-0.015	-0.006	-0.000	-0.010
11	-0.036	-0.029	-0.003	-0.019	+0.003

- **Interchip colour shifts** were detected in all CFH12K fields-of-view. For consistency in the data reduction of pre-main-sequence open clusters, the CCD04 was chosen as reference (the $I-z$ colour shift for this chip is always 0.0 mag). Tables 4.7, 4.8, and 4.9 list the shifts found for each individual chip in all five CFH12K field-of-view compared to CCD04 for the short, medium, and long exposures, respectively. Negative and positive values correspond to blue and red shifts in the $I-z$ colour to align properly all colour-magnitude diagrams with respect to CCD04. No clear trend was obvious for each individual chip besides that all of them need to be blue-shifted, except CCD05 and CCD06
- **Field-to-field colour shifts** were detected as well in all open cluster observations. Although fields A, B, and C were obtained on the same night and under photometric conditions, the $I-z$ colour did not align on top of each other. We choose field A as reference for the data in Collinder 359. We have applied colour shifts of +0.100, +0.010, +0.130, and +0.030 to the short exposures of fields B, C, D, and E, respectively, to align their colour-magnitude diagrams with respect to field A. We have applied colour shifts of -0.090, +0.010, -0.060, and -0.020 to the medium exposures and shifts of +0.030, +0.050, -0.010, and -0.020 to the long exposures of fields B, C, D, and E, respectively.
- **Exposure-to-exposure colour shifts** were detected as well in all CFH12K observations. After correcting for interchip and field-to-field discrepancies, we expected the colour-magnitude diagrams of the short, medium, and long exposures to align properly. However, $I-z$ colour shifts of -0.050, +0.030, and +0.020 for the short, medium, and long exposures, respectively, were still needed to correct for the difference.

After applying all colour shifts as described above, the $I-z$ colours are correct relative to a reference frame (in our case CCD04 of field A for short exposures) but the individual I and z magnitudes are in error by up to 0.10 mag, depending on the offset (Table 4.7, 4.8, and 4.9).

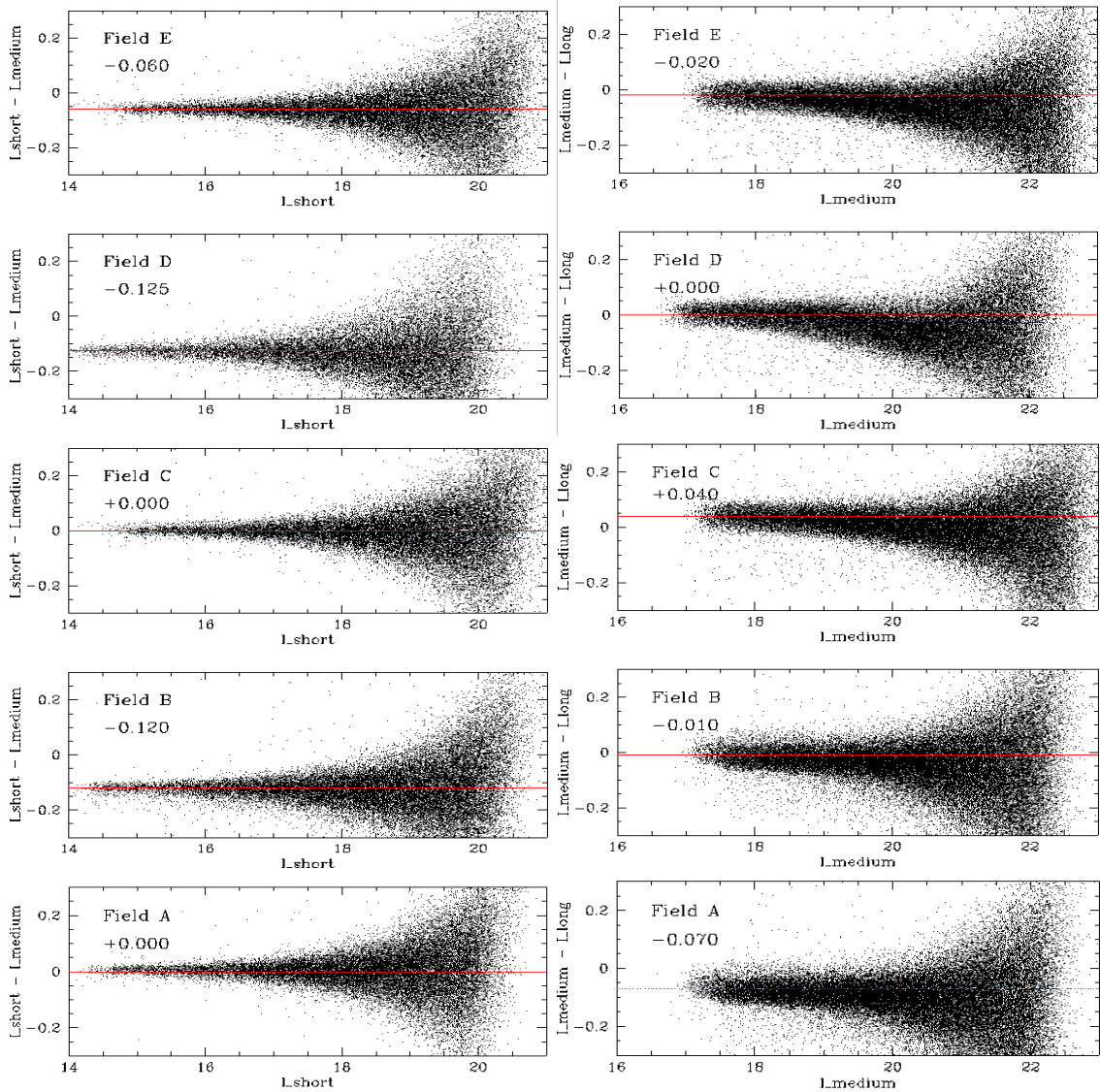


Figure 4.4: Differences in I magnitudes observed between the short and medium (left panels) and medium and long (right panels) exposures. From bottom to top are shown offsets for fields A, B, C, D, and E, respectively. Offsets are indicated in each panel and are represented by the lines.

This level of accuracy is certainly good enough for the selection of subsequent cluster member candidates.

To calibrate internally the I -band photometry, we have cross-correlated the short with medium and medium with long exposures for each individual field-of-view. Figure 4.4 displays the shift in I magnitude between the short and medium (left panel) and the medium and long (right panel) exposures, respectively. We have found offsets of +0.000, -0.120, +0.000, -0.125, and -0.060, between the short and medium exposures of fields A, B, C, D, and E, respectively. We have found

offsets of -0.070 , -0.010 , $+0.040$, $+0.000$, and -0.020 , between the medium and long exposures of fields A, B, C, D, and E, respectively. We could not calibrate the I magnitude between the five CFH12K fields-of-view since no overlapping region was available (Figure 4.2).

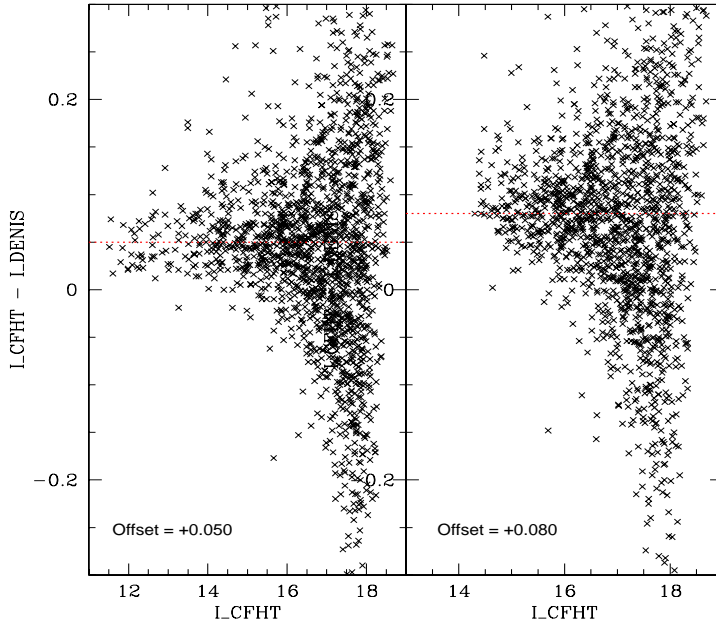


Figure 4.5: Offsets in I magnitudes between the CFHT and DENIS measurements for a $15' \times 6'$ overlapping area located in field A. Photometric shifts of $+0.050$ and $+0.080$ are found for the short (left panel) and medium (right panel) exposures, respectively. The same procedure was not possible with the long exposures since the detection of DENIS corresponds to the saturation limit of the CFH12K long exposures.

Comparison of the I magnitudes with measurements available in the literature for known cluster members was necessary to calibrate externally the I -band photometry. However, first, the CFH12K fields-of-view were chosen to avoid the bright components of the cluster (Figure 4.2), and, second, this cluster was fairly unstudied so that no known member is available in the surveyed area. Thus, we are not in a position to apply this method to the pre-main-sequence cluster Collinder 359. However, we have cross-correlated the final catalogue with the recent release of the DEep Near-Infrared Survey (Epchtein et al. 1997). The DENIS project is a deep astronomical survey of the Southern Sky in one optical band (I at $0.8\mu\text{m}$) and two near-infrared bands (J at $1.25\mu\text{m}$ and K at $2.16\mu\text{m}$) carried out with a one-meter telescope at La Silla (Chile). The whole Southern Sky is covered up to a declination of $+2^\circ$ down to $I = 18.5$, $J = 16.5$, $K_s = 13.5$. We could, therefore, extract a small overlapping region between the DENIS survey and the area covered by Field A. The right ascension and declination (J2000) of the $15' \times 6'$ overlapping area are:

$$\begin{array}{lclcl} 17:59:30 & \leq & \text{RA} & \leq & 18:02:30 \\ +01:54:00 & \leq & \text{Dec} & \leq & +02:00:00 \end{array}$$

The photometric offsets in the I magnitudes between the CFHT and DENIS measurements are +0.050 and +0.080 for short and medium exposures, respectively. Figure 4.5 shows the difference in I magnitudes between the CFHT and DENIS photometry versus the CFHT magnitudes for the short (left panel) and the medium (right panel) exposures, respectively. A similar procedure could not be applied to the long exposures because the DENIS detection limit corresponds to the saturation of the CFH12K long exposures ($I = 18.0\text{--}18.5$).

After both internal and external calibration of the photometry and colours, the final magnitudes given in the output catalogues are calibrated and the error on the I magnitudes should be of order 0.1 mag. However, no errors on the I and z magnitudes were computed by the PSFex software and we assume this uncertainty for the forthcoming analysis. The photometric errors could be extracted from overlapping regions but none is available in Collinder 359. The z magnitudes listed in the various tables throughout this chapter and in appendix are in error because the I magnitude was calibrated and colour shifts applied. However, the I –(I – z) values are correct within an uncertainty of 0.1 mag.

4.3.4 The optical colour-magnitude diagram for Collinder 359

The final ($I, I-z$) colour-magnitude diagram is presented on Figure 4.6. It includes all detections in the 1.6 square degree area surveyed in the pre-main-sequence open cluster Collinder 359. The detection and completeness (dashed line) limits of the survey are estimated to $I \sim z \sim 24.0$ and 22.0, respectively. To create the final colour-magnitude diagram, we have cross-correlated the short with medium and medium with long exposures to remove common detections and keep the best photometry. Hence, the photometry of the objects with $I \leq 15.0$, $15.0 \leq I \leq 19.0$, and $I \geq 19.0$ is extracted from the short, medium, and long exposures, respectively.

Overplotted on the colour-magnitude diagram are the NextGen (solid line; Baraffe et al. 1998), Dusty (dashed line; Chabrier et al. 2000b) and Cond (dotted line; Chabrier et al. 2000b) isochrones for 80 Myr, assuming a distance of 500 pc for the cluster (this distance is found to be the most likely; see § 4.5). The horizontal dashed line at $I \sim 20.0$ corresponds to the stellar/substellar boundary at $0.075 M_{\odot}$. The mass scale (in M_{\odot}) is indicated on the right-hand side of the plot and ranges from $1.3 M_{\odot}$ down to $0.030 M_{\odot}$. The large filled dots characterise all optically-selected cluster member candidates selected up to a distance of 650 pc for an age of 80 Myr to take into account the largest distance estimate from the literature (§ 4.2). The open triangles are cluster member candidates common to the Zacharias (2003) catalogue and consistent with the mean proper motion of the cluster. A reddening vector with $A_V = 1$ is indicated by an arrow for comparison purposes. We have considered the interstellar absorption law from Rieke & Lebofsky (1985), namely $A_I = 0.482$ for the I -band. As no estimate is available in the z band, we have assumed a linear fit between the interstellar absorption in the I and J bands ($A_J = 0.282$), yielding a value of $A_z = 0.382$.

4.3.5 Selection of cluster member candidates

The extraction of the cluster member candidates in open clusters generally consists in selecting objects located to the right of the ZAMS (Leggett 1992) shifted to the distance of the cluster. We have chosen the evolutionary models from the Lyon group to select cluster member candidates in Collinder 359. We have used the NextGen isochrones (solid line in Figure 4.6; Baraffe

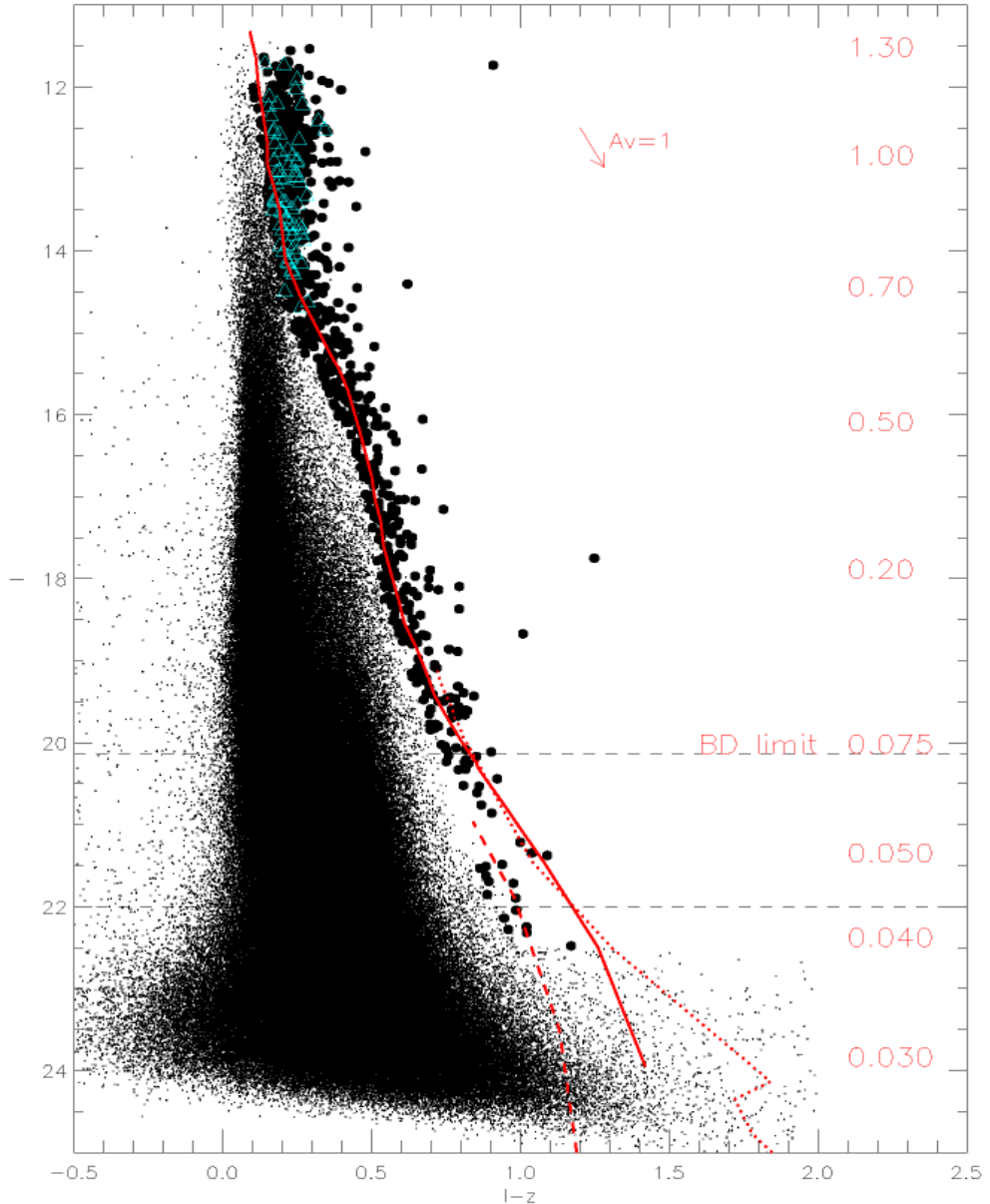


Figure 4.6: Colour-magnitude diagram ($I, I-z$) for the intermediate-age open cluster Collinder 359 over the full 1.6 deg^2 area surveyed by the CFH12K camera. The large filled dots are all optically-selected cluster member candidates spanning $1.30-0.04 M_\odot$. Overplotted are NextGen (solid line; Baraffe et al. 1998), the Dusty (dashed line; Chabrier et al. 2000b) and the Cond (dotted line; Chabrier et al. 2000b) isochrones for 80 Myr, assuming a distance of 500 pc for the cluster. The dashed line at $I \sim 20$ indicates the stellar/substellar boundary at $0.075 M_\odot$. The mass scale (in M_\odot) is given on the right side of the graph. A reddening vector of $A_V = 1$ is indicated for comparison purposes. The open triangles depict candidates with proper motion consistent with cluster membership.

et al. 1998) for effective temperatures higher than 2500 K (corresponding to masses of $0.050 M_{\odot}$ at the age and distance of the cluster) and the Dusty (dashed line in Figure 4.6; Chabrier et al. 2000b) isochrones for lower temperatures (and masses). We did not consider the Cond models (dotted line in Figure 4.6; Chabrier et al. 2000b) since the isochrone lie to the right of the Dusty isochrone. Consequently, objects located to the right of the Cond isochrones are to the right of the Dusty isochrones as well and, hence, remain bona-fide cluster member candidates.

We have considered three different values for the age of the cluster. First, an age of 30 Myr which corresponds to the value quoted in the Open Cluster Database. Next, an age of 50 Myr, and, finally, an age of 80 Myr to take into account uncertainties in the age determination of open clusters. There is, indeed, typically a factor of two between the age estimate from the turn-off main-sequence fitting (Mermilliod 1981) and the age determination based on the lithium test (Re-bolo et al. 1992). For example, the age of the Pleiades increased from 70 Myr to 125 Myr after applying the lithium test (Stauffer et al. 1998). Concerning α Per, the age increased from 50 Myr to 90 Myr (Stauffer et al. 1999; Chapter 3). Larger uncertainties are foreseen for unstudied open clusters such as Collinder 359.

The second uncertain parameter of Collinder 359 is the distance. From the literature search presented in § 4.2, distances range from 200 pc from the Open Cluster Database to 650 pc for the latest estimate by N. Kharchenko et al. (2004; personal communication). Early estimates of the distance by Collinder (1931) are within this interval. Isochrone fitting suggests a mean distance of 450 pc.

To take into account the uncertainties in the age and the distance of the cluster, we have selected *all* objects located to the right of the combined NextGen+Dusty isochrones (Baraffe et al. 1998; Chabrier et al. 2000b), shifted to distances from 250 pc to 650 pc by intervals of 50 pc and assuming three different ages (30, 50, and 80 Myr). This procedure has generated a total of 27 catalogues, each of them corresponding to a specific (distance, age) combination. The number of objects in each file is given in the Table 4.10 (§ 4.4.5). These files will be available on CDROMs upon request or in a webpage dedicated to Collinder 359. We have implemented the selection independently for the short, medium, and long exposures. Then, we have cross-correlated those catalogues to remove multiple detections and provide a list of cluster member candidates (Table B.1 in Appendix B). According to these conservative limits, we have certainly included the majority of true cluster members at the expense of a higher contamination.

We have examined each cluster member candidate by eye both in the I and z images to reject extended objects, blended sources, and detections affected by bad pixels or bad columns. Indeed, more than two-thirds of the objects located to the right of the evolutionary models were affected by bad pixels in one filter at least, or located on a bad column despite the good cosmetics of the CFH12K camera. The number of candidates, divided into short, medium, and long exposures (including the common ones), is as follows.

- 737 candidates extracted only in the short exposures
- 100 common candidates to the short and medium exposures
- 13 common candidates to the short, medium, and long exposures
- 102 candidates found only in the medium exposures

- 29 common candidates to the medium and long exposures
- 52 candidates extracted only in the long exposures

After removal of all spurious detections, the final list of cluster members contains a total of 1033 candidates ranging from $I = 12.0$ to $I = 22.5$ over 1.6 deg^2 area surveyed in Collinder 359. From the colour-magnitude diagram ($I, I-z$), the large field contamination at magnitudes brighter than $I \sim 15$ is clearly visible. Out of the 1033 candidates, about 60 % of them lie in the range $I = 12\text{--}15$. The contamination at brighter magnitudes (and thus at high masses) originates from the merging between the cluster sequence and the sequence of field stars. As a consequence, the large majority of candidates extracted in this part of the colour-magnitude diagram are mostly contaminants. The subsequent luminosity function (§ 4.5) and mass function (§ 4.6) are therefore biased at high masses. Additional observations are required to estimate the level of contamination in this part of the diagram. For comparison, the number of objects found in the medium and long exposures is similar to the number of cluster candidates extracted from the (R, I) survey in α Per (Barrado y Navascués et al. 2002; Chapter 3).

All 1033 cluster member candidates are listed in Table B.1 in Appendix B with their coordinates, photometry and membership status. They are ordered by increasing right ascension. The details of the columns in Table B.1 are given in Appendix B. Additional parameters, including the pixel (x,y) coordinates, ellipticity, full-width-half-maximum of each candidate will also be available upon request. The range of ellipticities and FWHM for all candidates are, 0.001–0.389 and 1.6–3.5, respectively. Only one object has an ellipticity of 0.602 and a FWHM of 4.0, casting doubt about its membership. The distribution of the ellipticity shows that 95 % of the objects have an ellipticity smaller than 0.15. The majority of objects have full-width-half-maximum between 1.8 and 3.0, corresponding to a seeing varying approximately between 0.4 and 0.6 arcsec. The seeing values are better than those requested in the CFHT proposal (0.65–0.8 arcsec).

All tables corresponding to the various (distance, age) combinations will be saved on CDROMs. Only the whole sample of candidates is provided in Appendix B as paper version. Appendix C provides one example of finding charts for candidates candidates in Collinder 359. The remaining finding charts will be available on CDROMs or available on a dedicated webpage.

We are confident that we have extracted most of the cluster member candidates in Collinder 359. However, inherent uncertainties to the selection procedure remain. We have possibly missed some bona-fide cluster members for various reasons. First, 200 bad columns affect the CFH12K field-of-view and most especially the CCD05. The largest incompleteness is expected in this specific chip. Second, objects affected by bad pixels might actually be genuine cluster candidates but were rejected from the final list. Next, blended objects were removed from the candidate list because their photometry was affected. Finally, some bright stars might hide faint cluster members although the short exposures were obtained to partly address this issue.

Figure 4.7 shows the distribution of all probable (Y+) cluster member candidates in the five CFH12K fields-of-view for a distance of 500 pc and an age of 80 Myr. The number of selected candidates is much lower in fields B and D than in the other three fields. We have found 169, 63, 105, 33, and 182 candidates in the field A, B, C, D, E, respectively. This plot is independent of the completeness limit of our survey as it happens above $I = 22.5$ mag. Using strong constraints in the FWHM and ellipticity for all detections in each individual CFH12K field-of-view, we have investigated the number of detections within one CFHT12K field-of-view:

- 94233 ± 934 objects in field A

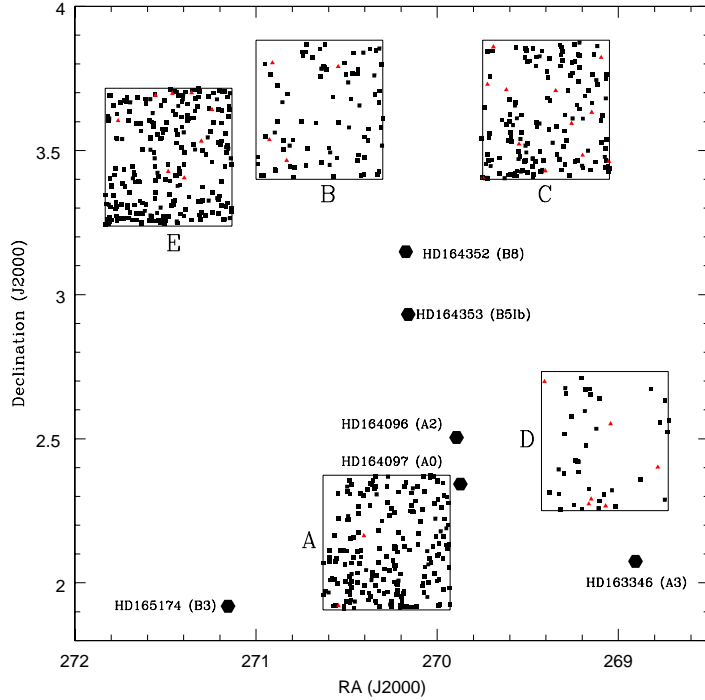


Figure 4.7: Distribution of the probable member candidates in the 1.6 square degree area in Collinder 359, assuming a mean distance of 500 pc and an age of 80 Myr. Six bright stars listed as cluster members by Collinder (1931) are included to facilitate the comparison with Figure 4.2.

- 118018 ± 812 objects in field B
- 99071 ± 467 objects in field C
- 81714 ± 331 objects in field D
- 111868 ± 506 objects in field E

The difference in density for cluster member candidates in Collinder 359 does not follow the difference in the total number of detections. The field D appear much less dense than the other fields. However, field B is as dense as field E in terms of detections but not with regard to the number of candidates. Fields A and C are comparable in density. The difference in density might result from a non-uniform extinction along the line of sight. Collinder 359 is located in the Aquila Rift, where CO maps indicate the presence of extinction (Dame et al. 2001).

It would be premature to explain this effect as a result of dynamical evolution within the cluster as optical spectroscopy and additional membership criteria are lacking. However, this issue certainly requires special attention in the near future and should be further investigated once the cluster sequence is better defined.

4.4 Near-infrared follow-up of optically-selected candidates

Collinder 359 is at a galactic latitude of $b = +12.5^\circ$, intermediate between α Per ($b = -7^\circ$) and the Pleiades ($b = -24^\circ$). Therefore, the sample of optically-selected cluster member candidates in Collinder 359 is inevitably contaminated by foreground and background objects. The possible sources of contamination are:

1. Galaxies
2. Reddened background giants
3. Field dwarfs

As special care was taken to remove extended objects from the cluster candidate list, the contamination by galaxies should be extremely small. Moreover, reddened background giants could be well rejected using an optical-to-infrared colour-colour diagram as described in the case of α Per (Section 3.5.6 and Figure 3.10). The last but not least, field dwarfs represent another source of contamination as they have similar optical colours as young cluster members. However, optical-to-infrared colour-magnitude diagrams such as $(I, I-J)$ or $(I, I-K)$ have proven their efficiency to weed out field dwarfs in σ Orionis (Zapatero Osorio et al. 2000), in the Pleiades (Zapatero Osorio et al. 1997a; Pinfield et al. 2000), in α Per (Barrado y Navascués et al. 2002), and in IC2391 (Barrado y Navascués et al. 2001a). Furthermore, the latest theoretical Dusty isochrones (Chabrier et al. 2000a) predict bluer $I-K$ colours for field dwarfs than young low-mass cluster members by 1.0 to 1.5 mag depending on the mass.

Near-infrared observations provide good means to weed out contaminating objects from the optical sample. This section is dedicated to the near-infrared follow-up of the optically-selected cluster member candidates in Collinder 359 extracted in the previous section. First, the list of cluster members was cross-correlated with the 2MASS all-sky survey database for objects brighter than $I = 17.0$ (§ 4.4.1). Next, near-infrared (K -band) follow-up observations, conducted with the Canada-France-Hawaii Telescope, for a sample of 39 cluster member candidates are described in § 4.4.2. The data reduction and analysis of the near-infrared images are presented in § 4.4.3 and § 4.4.4, respectively. The contamination of the optical sample is discussed in § 4.4.5.

The work presented in this section was done in collaboration with members from the Arcetri, Grenoble, and Potsdam teams, within the framework of the CFHT Key Programme and EC network. David James and Jérôme Bouvier carried out the observations at CFHT in visitor mode and Jérôme Bouvier reduced the infrared data. Willem-Jan de Wit, David James and I extracted the infrared photometry of the cluster member candidates in the IC4665, Steph 1, and Collinder 359 pre-main-sequence open clusters, respectively.

4.4.1 Cross-correlation with the 2MASS database

To estimate the contamination towards bright member candidates in Collinder 359, we have cross-correlated the sample of optically-selected cluster member candidate with the 2MASS survey. Information concerning the 2MASS all-sky survey and the catalogue products can be found in Beichman et al. (1998) as well as on the 2MASS webpage¹¹. A short overview of the 2MASS project is given in Chapter 1 (§ 1.5.2). Due to its completeness limit of $K_s = 14.3$, the 2MASS

¹¹<http://www.ipac.caltech.edu/2mass/releases/second/doc/>

database provides infrared counterparts in J , H , and K_s for most of the optically-selected cluster candidates brighter than $I = 17.0$. For objects fainter than $K_s = 14.3$, the uncertainty on the magnitude become larger than 0.1 mag and additional near-infrared observations are required to establish membership.

Among 805 cluster member candidates brighter than 17.0 in the I -band, 772 of them have a 2MASS counterpart within a radius of $2''$, with K_s magnitudes brighter than 14.3, and errors on the J , H , and K_s magnitudes smaller than 0.1 mag. These criteria did not allow the identification of 33 cluster member candidates in Collinder 359. Those objects have a 2MASS counterpart but either at larger radii (2 to $3''$) or K_s magnitudes fainter than 14.3 or uncertainties larger than 0.1 mag. We have therefore not taken into account their 2MASS magnitudes.

A radius of $2''$ is adapted to the selected cluster members as we examined those objects not to be blended with other stars in the field. For comparison, we used radii of about 1.5 and $1''$ to cross-correlate the optical and near-infrared catalogues in α Per (Sect 3.5.4). As only 33 objects were not identified during the matching, our sample of cluster member candidates with near-infrared counterparts in Collinder 359 is complete to 96 %. The subsample of cluster member candidates with 2MASS counterparts is displayed as plus symbols in Figure 4.8.

4.4.2 The CFHT K -band follow-up

Near-infrared (K' -band) observations of 39 optically-selected cluster member candidates were carried out with the infrared camera (CFHTIR) mounted on the Canada-France-Hawaii 3.6-m telescope on 10–12 July 2003 (Table 4.11). The observations were conducted by David James. The conditions were non-photometric over the three night observing run and the seeing around 0.5–0.7 arcsec. A second observing run was granted in November 2003 with the same infrared camera on CFHT. The observer was Jérôme Bouvier. The conditions were highly non-photometric and none of the five observed fields in Collinder 359 was usable to achieve the photometric accuracy better than 0.1 mag.

The CFHTIR infrared camera has a 1024×1024 pixel HAWAII detector with a spatial scale of $0.204''/\text{pixel}$ yielding a $3.5' \times 3.5'$ field-of-view. Five dithered frames (offset by ~ 50 pixels) were obtained for each target, each frame being a co-add of 7 or 8 images exposed 8 seconds, yielding a total exposure time on the order of 5 minutes. All observations were pointed observations as the candidates are randomly distributed over large areas. By chance, two or more objects were sometimes within one CFHTIR field-of-view. In total, we have observed K' -band photometry of 39 candidates in Collinder 359, spanning $I = 17.0\text{--}22.0$ to probe the contamination across the stellar/substellar boundary in the cluster. The error on the K -mag is better than 0.1 mag (see column 7 in Table 4.11).

Many CFHTIR fields contain bright cluster members as well but those are generally saturated. Hence, we retained the 2MASS photometry for the objects brighter than $I = 17.0$. Several standard stars (AS30, AS31, AS33; Table 4.12; Hunt et al. 1998) were observed throughout the nights to calibrate the zero-points. the achieved accuracy is on the order of 0.02 mag. Series of dome flat-fields (light on and off) were taken before the beginning of the night to correct pixel-to-pixel variations.

Table 4.11 lists the 39 optically-selected cluster member candidates followed-up in the K' -band with the CFHTIR camera. Two objects, brighter than $I = 17.0$, are among the objects whose 2MASS magnitudes were rejected. Columns 1 and 2 list the identification number of the target

Table 4.11: List of optically-selected cluster member candidates in Collinder 359 with infrared follow-up obtained with the CFHTIR camera. The objects are sorted by decreasing I magnitudes. Column 1 provide the name according to the IAU convention, starting with Coll359 J and followed by the coordinates. Columns 2 and 3 give the field and the CCD where the object is located. Columns 4, 5, and 6 lists the I , z magnitudes, and $I-z$ colour, respectively. Columns 7 and 8 gives the K' magnitude along with its associated error and the $I-K'$ colour. Column 9 gives the membership status based on the optical-to-infrared colour-magnitude diagram.

Coll359 J ...	Field	ID	I	z	$I-z$	$K' \pm \text{err}K'$	$I-K'$	Memb?
180432+031617	E06	250	14.800	14.490	0.310	13.328 ± 0.003	1.472	Y?
180511+032221	E07	2225	16.667	16.159	0.508	14.325 ± 0.005	2.342	Y+
180553+033510	E02	2089	17.044	16.551	0.493	14.743 ± 0.006	2.301	Y+
180009+022152	A00	153	17.246	16.689	0.557	14.842 ± 0.007	2.404	Y+
180045+020257	A08	2038	17.465	16.932	0.533	14.913 ± 0.999	2.552	Y+
180000+022159	A00	95	17.484	16.843	0.641	14.934 ± 0.007	2.550	Y?
180548+033619	E02	1774	17.548	16.902	0.646	15.008 ± 0.008	2.540	Y?
175743+032953	C09	1239	17.600	17.048	0.552	15.055 ± 0.008	2.545	Y+
180343+033137	B11	3969	17.720	17.106	0.614	15.033 ± 0.007	2.687	Y?
180032+020711	A07	2501	17.752	17.148	0.604	15.438 ± 0.009	2.314	Y?
180551+031550	E08	439	17.778	17.076	0.702	15.471 ± 0.011	2.307	Y?
175852+033359	C11	1971	17.857	17.164	0.693	15.158 ± 0.009	2.699	Y?
175458+021734	D06	271	17.997	17.267	0.730	15.026 ± 0.007	2.971	Y?
180147+032650	B07	565	17.998	17.306	0.692	15.651 ± 0.010	2.347	Y+
175728+033036	C08	1509	18.140	17.482	0.658	15.315 ± 0.008	2.825	Y?
180520+032123	E07	4232	18.166	17.555	0.611	15.605 ± 0.011	2.561	Y?
180351+032945	B11	2938	18.234	17.675	0.559	15.615 ± 0.010	2.619	Y+
175725+033117	C08	1676	18.442	17.679	0.763	15.744 ± 0.011	2.698	Y?
180004+022210	A00	201	18.674	17.666	1.008	14.895 ± 0.007	3.779	Y+
180549+031530	E08	523	18.945	18.236	0.709	16.355 ± 0.019	2.590	Y?
180022+021436	A01	3978	19.007	18.161	0.846	15.657 ± 0.011	3.350	Y?
180554+031521	E08	418	19.260	18.515	0.745	16.720 ± 0.024	2.540	NM
180657+034026	E05	2197	19.336	18.348	0.988	16.962 ± 0.024	2.374	NM
175506+021710	D06	576	19.556	18.609	0.947	15.874 ± 0.011	3.682	Y?
180516+032036	E07	3671	19.630	18.948	0.682	17.069 ± 0.025	2.561	NM
180439+033421	E00	8531	20.020	19.232	0.788	17.787 ± 0.042	2.233	NM
180342+033213	B11	7730	20.257	19.432	0.825	16.793 ± 0.022	3.464	Y+
180656+033222	E05	10305	21.026	19.694	1.332	17.982 ± 0.055	3.044	NM
180305+035059	B03	1155	21.857	20.918	0.939	18.852 ± 0.067	3.005	NM
180702+033219	E05	10242	22.175	21.052	1.123	18.308 ± 0.093	3.867	Y?

according to IAU conventions. The CFH12K field and CCD number where the candidate is located are given in columns 2 and 3, respectively. The I , z , K' magnitudes and the $I-z$ and $I-K'$ colours are provided in columns 4–8. The membership status of the cluster member candidates in Collinder 359 is updated in the last column of Table 4.11. The Y+, Y?, and NM abbreviations refer to objects classified as probable, possible members and non-members, respectively.

4.4.3 Data reduction of the CFHT near-infrared images

Five dithered frames, offset by about 50 pixels ($\sim 10''$) were obtained for each science target. Each science frame is a sum of images, that is one FITS file saved on disk contains several images

Table 4.12: List of standard stars observed within the framework of the CFHTIR follow-up of selected cluster member candidates in three pre-main-sequence open clusters on 10–12 July 2003. Note that only standard stars bracketing the observations in Collinder 359 are listed. The remainder show similar zero-points converging to a mean value of $ZP = 22.90 \pm 0.02$.

Name	RA	DEC	Time	ExpT	Airm	K_{Hunt}	K'_{instr}	ZPs
10 June 2003								
AS30-0	16:40:41.6	+36:21:13	06h17	3.0 sec	1.112	13.141	15.255	22.886
AS30-1	16:40:41.6	+36:21:13	06h17	3.0 sec	1.112	12.175	14.155	23.020
AS31-0	17:44:06.8	-00:24:58	06h23	5.0 sec	1.335	12.048	14.144	22.904
AS31-1	17:44:06.2	-00:24:22	06h23	5.0 sec	1.335	12.476	14.614	22.862
AS33-0	18:27:13.6	+04:03:10	10h50	3.0 sec	1.100	11.739	13.826	22.913
AS33-2	18:27:12.4	+04:02:16	10h50	3.0 sec	1.100	13.168	15.286	22.882
AS33-0	18:27:13.6	+04:03:10	10h55	3.0 sec	1.100	11.739	13.826	22.913
AS33-2	18:27:12.4	+04:02:16	10h55	3.0 sec	1.100	13.168	15.336	22.832
11 June 2003								
AS30-0	16:40:41.6	+36:21:13	05h54	3.0 sec	1.145	13.141	15.309	22.832
AS30-1	16:40:41.6	+36:21:13	05h54	3.0 sec	1.145	12.175	14.189	22.987
AS31-0	17:44:06.8	-00:24:58	06h22	3.0 sec	1.324	12.048	14.160	22.888
AS31-1	17:44:06.2	-00:24:22	06h22	3.0 sec	1.324	12.476	14.620	22.856
AS33-0	18:27:13.6	+04:03:10	07h48	3.0 sec	1.149	11.739	13.822	22.917
AS33-2	18:27:12.4	+04:02:16	07h48	3.0 sec	1.149	13.168	15.292	22.876
AS31-0	17:44:06.8	-00:24:58	10h29	3.0 sec	1.182	12.048	14.185	22.863
AS31-1	17:44:06.2	-00:24:22	10h29	3.0 sec	1.182	12.476	14.610	22.866
12 June 2003								
AS30-0	16:40:41.6	+36:21:13	05h51	3.0 sec	1.142	13.141	15.243	22.898
AS30-1	16:40:41.6	+36:21:13	05h51	3.0 sec	1.142	12.175	14.173	23.002
AS31-0	17:44:06.8	-00:24:58	05h57	3.0 sec	1.425	12.048	14.233	22.815
AS31-1	17:44:06.2	-00:24:22	05h57	3.0 sec	1.425	12.476	14.633	22.843
AS33-0	18:27:13.6	+04:03:10	11h00	3.0 sec	1.130	11.739	13.844	22.895
AS33-2	18:27:12.4	+04:02:16	11h00	3.0 sec	1.130	13.168	15.343	22.824

(in this specific case 7 or 8) which were co-added to construct the final image. The data reduction was relatively standard for near-infrared observations and was carried out by Jérôme Bouvier. However, due to non-photometric conditions, we have tested three different methods to estimate the sky and achieve the best possible photometric accuracy. A brief outline is provided below:

- 1. Method 1: “standard”:** The sky was estimated by taking the median of the five dithered science field frames. As only 5 dithered frames were available to compute the sky, the final sky subtracted science images did exhibit “negative stars” in the background. These “negative stars” affect the real “stars” themselves and will flaw the photometry. Thus, we rejected this approach.
- 2. Method 2: “supersky”:** To get rid off the “negative stars”, a median images of 11 successive science frames with minmax rejection was used to create a “supersky”. The science

exposures corrected for the “supersky” nevertheless exhibit a non-uniform (low-level) background. The photometry will be correct as long as the sky is estimated locally around the stars. This method yields the highest signal-to-noise ratio as more frames were used to estimate the sky.

3. **Method 3: “skynorm”:** To get “nice-looking” images without “negative stars” and a uniform background, the sky was estimated from the five frames after having renormalised all of them to the same value. The median average of the normalised science image is a more meaningful sky estimate and do exhibit neither “negative stars” nor non-uniform background even during non-photometric conditions. The photometry measured on these images will also be correct, though probably lower signal-to-noise than method 2, because fewer frames (only five) were used to estimate the sky.

After estimating correctly the sky background, each science frame was sky-subtracted and flat-fielded. The flat-field is the difference between averaged flat fields observed lamp on and lamp off. Aperture photometry was done by myself within the IRAF environment and is described below.

The measured magnitudes were corrected for extinction and exposure time according to the equation below in order to obtain instrumental magnitudes.

$$m_{\text{instrumental}} = m_{\text{measured}} - \text{Extinction} \times \text{Airmass} + 2.5 \times \log(\text{ExpTime})$$

The airmass correction for CFHT on Mauna Kea was assumed to be 0.07 mag/airmass. The airmass and exposure time keywords were directly read from the header of the fits files. Zero-points from the various standards observed throughout the nights were applied to the instrumental magnitudes of the cluster member candidates to derive the final magnitudes. A list of standard stars along with their instrumental magnitudes as well as the derived zero-points is provided in Table 4.12. The mean zero-point for all three nights was $ZP = 22.90 \pm 0.02$ but variable during a night.

However, due to the non-photometry conditions encountered during the observing run, a cross-correlation with the 2MASS database was implemented to check the reliability of the photometric calibration. The task *daofind* was used to detect all sources on the science frames. The full-width-half-maximum, the sky level and the detection threshold were adjusted for each frame to detect all sources. The photometry was then computed with the task *phot*. An aperture on the order of the FWHM was chosen. The flux of few relatively bright and isolated stars was measured for different aperture sizes (from 1 to 4 times the FWHM) to compute the aperture correction. Each individual frame was astrometrically calibrated following the procedure described in Section 3.5.3. Then, we have cross-correlated the CFHTIR sources with the 2MASS database to compare both photometry. The differences in K magnitudes were in agreement with the zero-points derived from the standard stars within 0.05 mag.

The final calibrated magnitudes of the optically-selected cluster candidates in Collinder 359 are listed in Table 4.11 and displayed as filled circles in Figure 4.8.

4.4.4 Analysis of the CFHT observations

We have obtained near-infrared (K' -band) photometry for 39 optically-selected cluster member candidates in Collinder 359 (Table 4.11 and Figure 4.8). Those candidates span $I = 17.0\text{--}22.0$

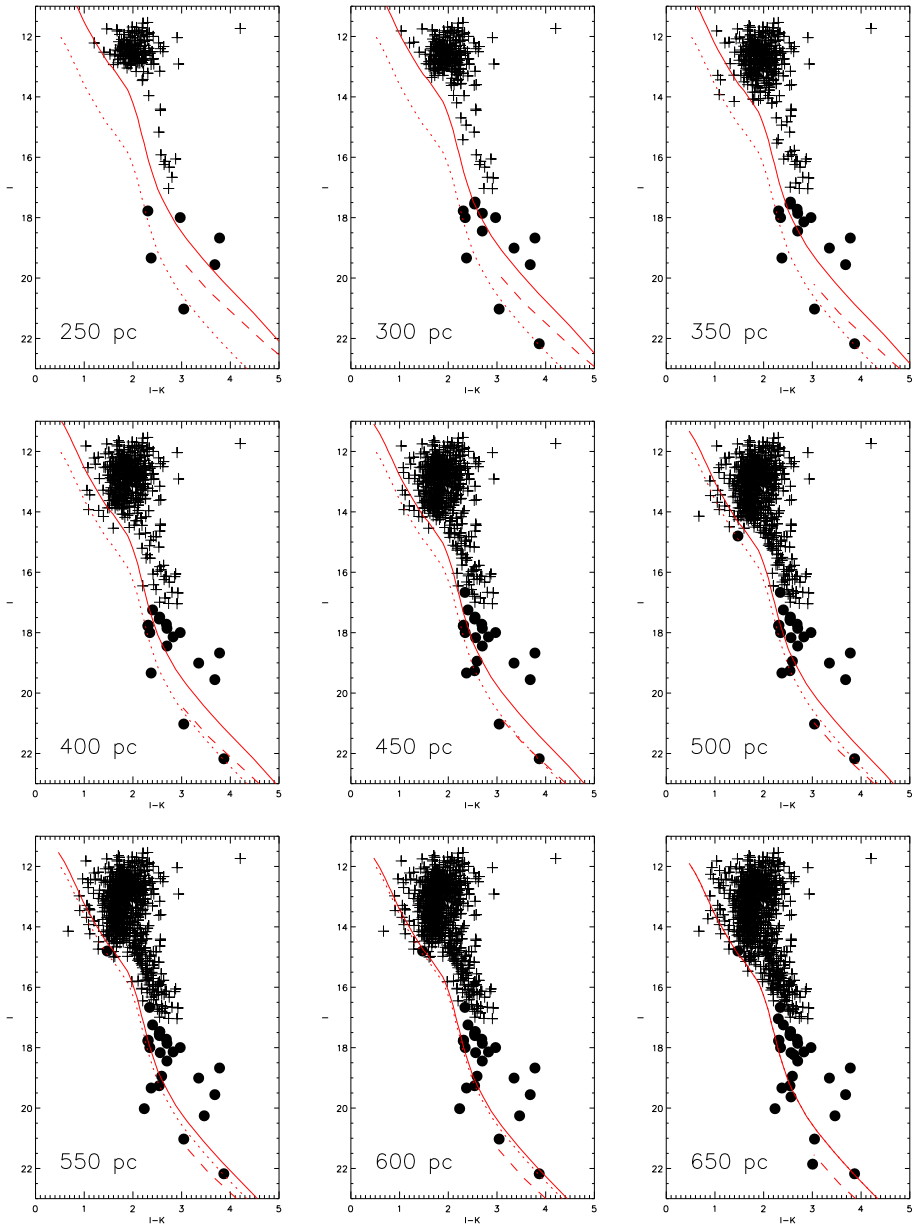


Figure 4.8: We plot in the $(I, I-K)$ colour-magnitude diagrams the cluster member candidates located to the right of the NextGen+Dusty isochrones in the $(I, I-z)$ diagram, shifted at distances ranging from 250 to 650 pc by intervals of 50 pc at an age of 80 Myr. The infrared photometry comes from the 2MASS catalogue from objects brighter than $I = 17$ (plus symbols) and from our CFHTIR follow-up observations for fainter objects (filled circles). Overplotted are the NextGen (solid lines) and Dusty (dashed lines) isochrones shifted at the distance indicated at the bottom left corner as well as the NextGen isochrone shifted at a distance of 650 pc (dotted line). Probable members ($Y+$) are objects located to the right of the isochrones shifted at the distance indicated in the diagrams. Possible members ($Y?$) are located to the right of the isochrones shifted at the indicated distance and the isochrone at 650 pc. The objects bluer than the isochrone shifted at 650 pc are rejected as cluster members.

mag and were specifically followed-up to probe the contamination across the hydrogen-burning limit as well as in the brown dwarf regime in pre-main-sequence open clusters. Two objects are brighter and one fainter than those limits. The brightest one, for which K' photometry has been obtained is added to the list of objects with 2MASS counterparts. The position of these candidates in the $(I, I-K)$ colour-magnitude diagram will add a further criterion to weed out contaminating objects from the list of cluster members. For example, at a given luminosity, a $0.04 M_{\odot}$ brown dwarf at 30 Myr has a $I-K$ colour of 3.8, while a $0.1 M_{\odot}$ star at 1 Gyr has a colour of 3.2 (Baraffe et al. 1998).

Figure 4.8 displays in optical-infrared ($I, I-K$) colour-magnitude diagrams the candidates selected to the right of the NextGen+Dusty isochrones in the $(I, I-z)$ diagram. Each diagram corresponds to a given distance, ranging from 250 to 650 pc by intervals of 50 pc. The infrared photometry was extracted from the 2MASS database for candidates brighter than $I = 17$ (plus symbols in Figure 4.8; Section 4.4.1). The fainter candidates have K' -band photometry from our CFHTIR follow-up observations (filled circles in Figure 4.8; Section 4.4.2). According to the location of the optically-selected cluster member candidates in the $(I, I-K)$ diagram and assuming an age of 80 Myr, three samples have been defined as follows:

1. Probable members (Y+): these objects lie to the right of the NextGen+dusty isochrones (solid and dashed lines), shifted at the distance indicated in the lower left corner in the diagram (distances ranging from 250 to 650 pc). Their optical and optical-to-infrared colours are consistent with cluster membership.
2. Possible members (Y?): these candidates are located between the NextGen+Dusty isochrones (solid and dashed lines) at the distance indicated in the diagram and the NextGen isochrone shifted at the distance of 650 pc (dotted line).
3. Non-members (NM): these objects are bluer than the NextGen isochrone shifted at the distance of 650 pc. They are rejected as cluster members.

Table 4.10 summarises the number of optical detections (all), probable (Y+) and possible (Y?) members, and non-members (NM) as well as the number of candidates with infrared photometry from 2MASS and from our CFHTIR observations for the various (distance, age) combinations. The membership of each individual object observed with CFHT is also given in the last column in Table B.1 in Appendix B. Out of 39 candidates observed with the CFHTIR camera, 8 remain probable candidates (Y+), 14 are possible members (Y?), and the remainder are classified as non-members (NM). For comparison purposes, we provide the number of objects present in the magnitude range $I = 12-15$, where the contamination is extremely high.

4.4.5 Contamination of the optical sample

The aim of this section is to estimate the contamination among the optically-selected cluster member candidates in Collinder 359. Combining the optical and optical-to-infrared colour-magnitude diagrams, most of the candidates brighter than $I = 17.0$ remain probable candidates. Indeed, 9 out of 805 are rejected as cluster members and 15 more are classified as possible members. Hence, the contamination appears to be on the order of 1–3 %. However, from the $(I, I-K)$ colour-magnitude diagrams (Figure 4.8), we can assess that the estimate above is a strict lower limit to the true contamination. A large bulk of stars brighter than $I = 15$ mag are likely very

red field stars contaminating the optical sample as discussed before. Ultimately, low-resolution spectroscopy will add further constraints to distinguish field stars from cluster members. The cluster sequence appears more pronounced for magnitudes fainter than about 15 and extends to fainter magnitudes. However, from the colour-magnitude diagrams, this sequence is less and less well-defined towards fainter magnitudes simply because near-infrared follow-up observations are lacking for the large majority (90 %) of candidates (only 39 were followed-up out of 359).

In Figure 4.9, we display the ($I-z, I-K$) colour-colour diagram of the optically-selected cluster member candidates with infrared magnitudes. The K magnitudes refer to K_s for objects with 2MASS counterparts ($I \leq 17.0$ mag) and to K' for fainter objects followed-up with the CFHTIR camera. The 50 % transmission edges of the K_s filter¹² lie at $2.31\,\mu\text{m}$ and $1.97\,\mu\text{m}$ whereas it is located at $2.0\,\mu\text{m}$ and $2.30\,\mu\text{m}$ for the K' filter¹³. The difference between both filters becomes important shortwards of $2.1\,\mu\text{m}$ as the K_s filter is narrower than the K' filter to minimise the contribution from the Earth atmosphere. We will consider here that the choice of the filter has little influence on the magnitude as no colour term was found in the course of our infrared study in α Per. As a consequence, the ($I-K$) colour and the membership assessment are not strongly affected by the difference in filters. However, this is likely to play a role for large optical-to-infrared colours.

In Figure 4.9, the solid line indicates the NextGen 50 Myr isochrone for masses larger than $0.1\,\text{M}_\odot$ and the Dusty 50 Myr isochrone for lower masses. The hook at $I-z \sim 0.65$ and $I-K \sim 2.5$ corresponds to $0.1\,\text{M}_\odot$ and reflects the difference in magnitudes derived from the NextGen and Dusty models. The NextGen model predicts an absolute I magnitude of 10.33 and whereas the Dusty model predicts $I = 10.51$ mag for a $0.1\,\text{M}_\odot$ star.

The ($I-z, I-K$) colour-colour diagram (Figure 4.9) does not provide any additional useful criterion for membership assessment. No clear cluster sequence emerges from this diagram due to, on the one hand, the large contamination at small ($I-K$) colour (plus symbols), and, on the other hand, the small number of objects with infrared magnitudes below $I = 17$ mag (filled circles). We nevertheless notice that the contamination originates mostly from field stars rather than giants, contrary to the results found in our study of α Per (Chapter 3).

To summarise, the optical selection method appears rather efficient at extracting cluster member candidates in Collinder 359 from the large number of contaminating objects detected in the CFH12K wide-field images. Infrared K' -band photometry was used to weed out contaminating field dwarfs at magnitudes fainter than about $I = 15$. for the bulk of objects brighter than this boundary, the optical-to-infrared colours are not sufficient to estimate the level of contamination. Additional near-infrared photometry of the remainder ~ 300 faint candidates is required to further analyse the contamination at and below the stellar/substellar boundary. A total of 8 nights was granted for K -band imaging in June 2004, divided into 4 nights with the 2.2-m telescope at Calar Alto and 4 nights with the CFHT 3.6-m telescope. Also time for low-resolution optical spectroscopy was granted with the TNG/DOLORES and WHT/AF2/WYFFOS spectrographs to assign spectral types to the optically-selected cluster member candidates in Collinder 359 and ascertain membership.

¹²http://www.ipac.caltech.edu/2mass/releases/allsky/doc/sec6_4a.tbl3.html

¹³<http://www.cfht.hawaii.edu/Instruments/Filters/curves/cfh5338.dat>

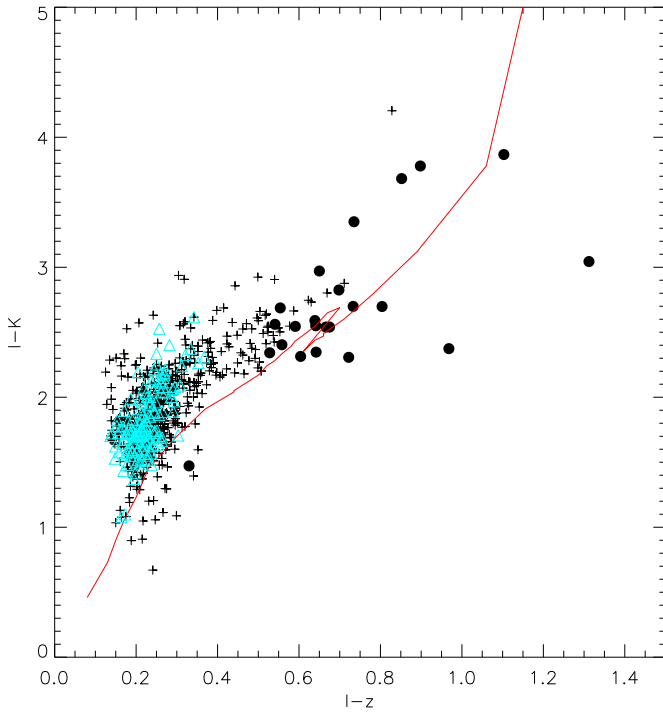


Figure 4.9: $(I-z, I-K)$ colour-colour diagram for the cluster member candidates in Collinder 359 with infrared magnitudes. The photometry is derived from the 2MASS database for objects brighter than $I \leq 17$ mag (plus symbols) and from the CFHTIR follow-up obtained in July 2003 for fainter objects (filled circles). The open triangles indicate candidates with proper motion (UCAC2; Zacharias et al. 2003) consistent with cluster membership. The solid line corresponds to the NextGen 50 Myr isochrone for masses above $0.1 M_{\odot}$ and the Dusty 50 Myr isochrone for lower masses. The hook reflects the difference in magnitudes predicted by the NextGen and Dusty isochrones for a $0.1 M_{\odot}$. Most of the contaminants are likely field dwarfs and not background giants seen along the line of sight of the cluster.

4.5 The luminosity function of Collinder 359

As discussed earlier, the age and distance estimates for Collinder 359 are poorly constrained. Collinder 359 has not been studied extensively to date and the wide-field optical survey presented in this thesis is the first of this kind for the cluster. Thus, we would like to address in this section three major issues regarding the cluster, which are of prime importance in inferring its luminosity function.

1. Can we confirm the existence of the cluster?
2. What is the age of the cluster?
3. What is the distance of the cluster?

4.5.1 The existence of the cluster

According to the available literature on Collinder 359, a handful of objects belong to the cluster, we are confronted to the following question: can we confirm the existence of the cluster? Optical images of the region around 67 Oph do not show an obvious clustering as for the Pleiades as reported by Melotte (1915) and Collinder (1931). Despite the intermediate galactic latitude ($b = +12.5^\circ$) of Collinder 359 between the α Per and the Pleiades clusters, the gap between field stars and cluster members is not evident in the $(I, I-z)$ colour-magnitude diagram (Figure 4.6). Furthermore, no clear cluster sequence stands out in this diagram to infer the presence of a cluster.

To address this issue, we have used proper motion information from the second release of the on-going USNO CCD Astrograph Catalog (hereafter UCAC2) project. Another source of proper motions for the cluster is the SuperCOSMOS Sky Survey database. However, plates north of $+2^\circ$ in declination are being processed and scanned at the moment and will be available only in summer 2004 over the entire cluster area (N. Hambly, personal communication).

The UCAC2 is a high density and highly accurate astrometric catalogue of over 48 million stars covering the sky from -90° to $+40^\circ$ in declination (Zacharias et al. 2003). The observed positional errors are about 20 mas for stars brighter than 14 mag and of order 70 mas for stars down to 17.0 mag. The photometry is provided in a non-standard filter located between the V and R filters. The magnitudes suffer from large uncertainties up to 0.3 mag but are not of interest within the framework of this study. We have extracted from the UCAC2 database the coordinates (J2000) and proper motions for all objects within one degree in radius from the cluster centre (RA = $18^{\text{h}}02^{\text{m}}$ and Dec = $+02^\circ 54'$) to the faintest magnitude available.

Figure 4.10 displays the vector point diagrams (proper motion in right ascension versus proper motion in declination) for all stars within one degree in radius from the cluster centre for magnitude brighter than 10.0, 11.0, 12.0, and 13.0, respectively. Two clustering of stars emerge from vector point diagrams where objects brighter than 12.0 mag are included. Two peaks are seen as well when plotting the number of stars as a function of declination. The first group of stars has no significant proper motion and denotes field stars whereas the second exhibits a shift in declination and corresponds to the cluster. The proper motion of the cluster is approximately 0.0 mas/yr and -8.5 mas/yr in right ascension and declination, respectively. The latter values are consistent with the proper motion of the star 67 Oph (*Hipparcos*; Perryman et al. 1997) and the various cluster motion estimates (Collinder 1931; Kharchenko et al. 2004). The separation between field stars and cluster members is hampered at fainter magnitudes by higher contamination so that both groups of stars become indistinguishable.

Based on the vector point diagrams with proper motion measurements for bright objects, **we conclude that the cluster exists and has a mean proper motion of approximately $(0.0, -8.5)$ mas/yr in right ascension and declination, respectively.**

4.5.2 The age of the cluster

Next, we attempt to derive an age for Collinder 359 using our wide-field optical survey and estimate the associated uncertainties. We have followed the approach applied to the α Per cluster by Stauffer et al. (2003). By comparing the location of the star α Persei (filled square in Figure 4.11) in the colour-magnitude diagram ($M_V, B-V$) with theoretical solar metallicity isochrones including moderate overshoot (Girardi et al. 2002), Stauffer et al. (2003) inferred an age of about 50 Myr

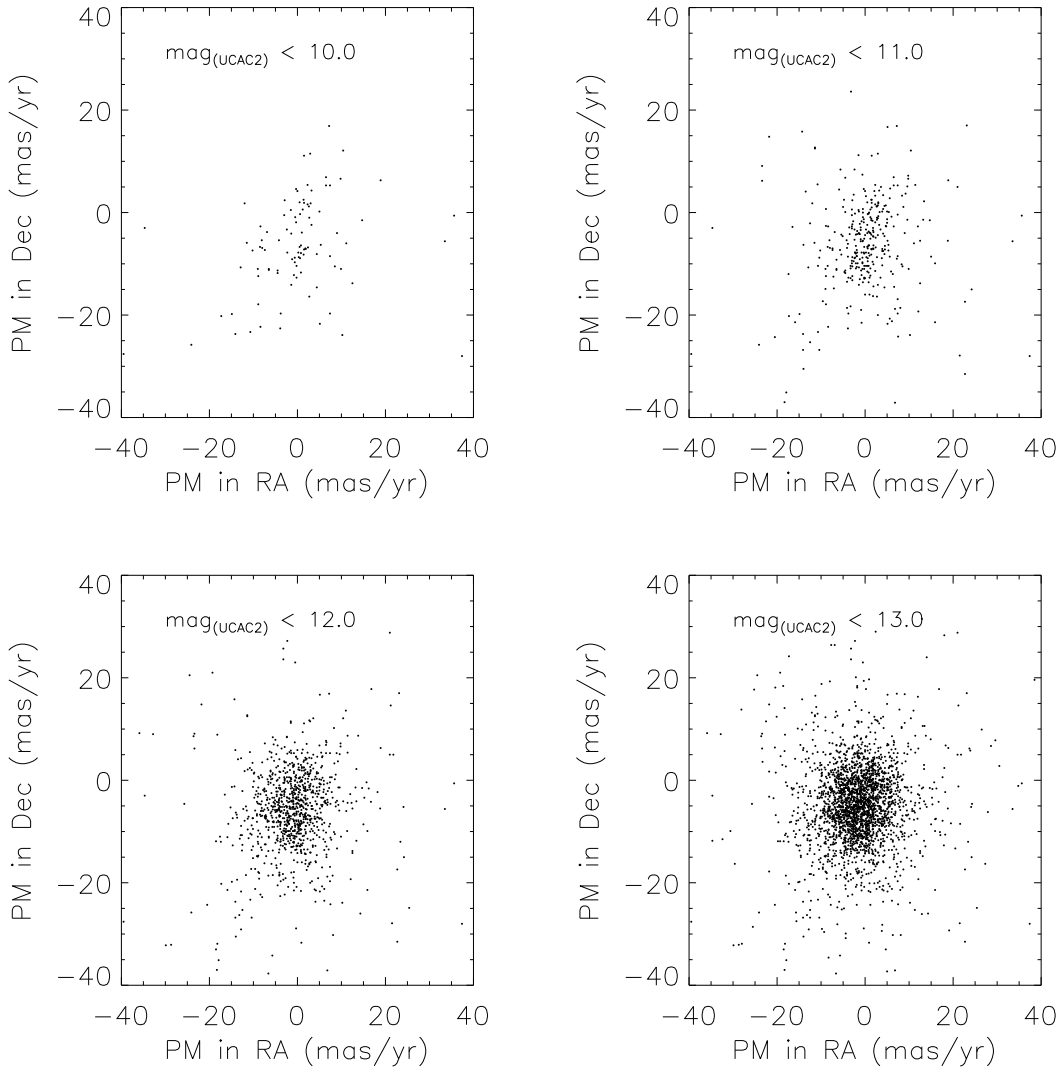


Figure 4.10: Vector point diagrams for all stars located within one degree in radius from the cluster centre for magnitudes brighter than 10, 11, 12, and 13 from left to right, respectively. The proper motions (accurate to 6 mas/yr) are taken from the USNO CCD Astrograph Catalog (Zacharias et al. 2003). Two groups of stars are clearly separated for magnitudes brighter than 12.0. The first is located at (0,0), and the second at approximately (0.0, -8.5) mas/yr in right ascension and declination, respectively. For fainter stars, both groups of stars are merged because of higher field star contamination.

for α Per (solid line in Figure 4.11). We should keep in mind here that the lithium test applied to the α Per cluster yielded a value twice larger than the turn-off main-sequence method (90 Myr versus 50 Myr; Stauffer et al. 1999).

Collinder 359 is located around the B5 supergiant, 67 Oph (filled hexagon in Figure 4.11), which is considered as a member of the cluster with a probability of 75 % and over 95 % by Baumgardt et al. (2000) and Kharchenko et al. (2004, personal communication), respectively. The Hipparcos parallax of 67 Oph is 2.30 ± 0.77 mas/yr and its proper motion 0.41 and -8.22 mas/yr in right ascension and declination, respectively (Perryman et al. 1997).

Assuming a mean apparent magnitude of $V = 3.97 \pm 0.02$ and a mean distance of 435^{+220}_{-110} pc (Perryman et al. 1997), we have derived an absolute magnitude of $M_V = -4.22^{+0.63}_{-0.89}$. The vertical line crossing the hexagon in Figure 4.11 represents the uncertainty on the parallax estimate of 67 Oph. The best positional fit of 67 Oph in the $(M_V, B-V)$ colour-magnitude diagram is obtained for an age of 60 Myr (between the solid and dotted lines in Figure 4.11), with an uncertainty of 20 Myr (extent of the vertical line). Our age estimate is twice as large as the 30 Myr age from

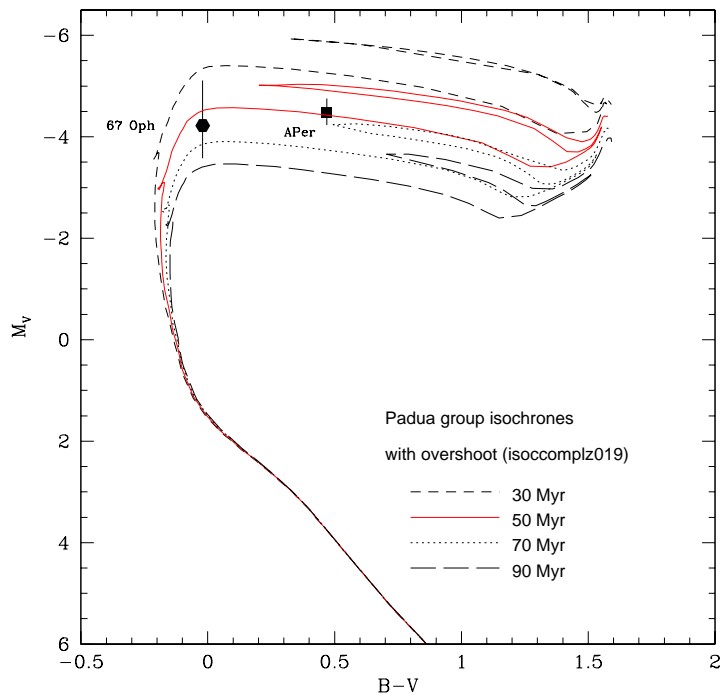


Figure 4.11: $(M_V, B-V)$ colour-magnitude diagram. The position of the F5 supergiant Alpha Per (filled square) and the B5 supergiant 67 Oph (filled hexagon) are indicated. Overplotted are the solar metallicity evolutionary models with moderate overshoot from the Padua group (Girardi et al. 2002) for 30 Myr (dashed line), 50 Myr (solid line), 70 Myr (dotted line), and 90 Myr (long dashed line). The vertical line crossing the solid hexagon represent the errors on the *Hipparcos* parallax measurement for 67 Oph (Perryman et al. 1997). The best fit is obtained for ages of 50 Myr and 60 Myr for the α Per and Collinder 359 clusters, respectively.

Wielen (1971) but comparable to the main-sequence turn-off age of the α Per cluster. Considering the increase in age from 50 Myr to 90 Myr for α Per, the age for Collinder 359 is likely to be older. Assuming a factor of ~ 1.6 between the age from the turn-off main-sequence and the lithium test as suggested by Jeffries & Naylor (2001), the value of age for Collinder 359 would go up to 100 Myr. In this study, we will consider the mean value of the two ages, namely 80 Myr. The lithium test is obviously needed in Collinder 359 to constrain further the age of the cluster.

Based on the present data available for the cluster, we conclude that Collinder 359 has an age estimate comparable to the α Per cluster in the range 60–100 Myr.

4.5.3 The distance of the cluster

Finally, we present a distance estimate for Collinder 359 using the proper motion information available from the UCAC2 catalogue. We have cross-correlated the optically-selected cluster member candidates from the CFH12K optical survey with the UCAC2 catalogue (Zacharias et al. 2003), using matching radii of four times the dispersion value of $0.553''$ and $0.320''$ in right ascension and declination, respectively. A total of 472 objects (open circles in Figure 4.12) were common to both catalogues between $I = 11.6$ and 15.1 mag, representing about 70 % of the whole optical candidate list within this magnitude range. The UCAC2 catalogue includes only the objects with proper motion information so that the 30 % of objects lacking could be explained by the incompleteness of the UCAC2 catalogue.

We have already mentioned the large field contamination at magnitudes brighter than $I = 15$. To minimise this contamination, we have selected from the vector point diagram (left panel in Figure 4.12) proper motion candidates located within a circle centred on the motion of 67 Oph (0.41 and -8.22 mas/yr; Perryman et al. 1997). The radius of the circle, chosen equal to 3.5 mas/yr in both directions, corresponds to the dispersion of the probable cluster members selected by Kharchenko et al. (2004, personal communication; open squares in Figure 4.2) to derive a distance of 650 pc and an age of 30 Myr for Collinder 359. The method employed by Kharchenko to extract members and determine the cluster is as follows. First, objects are selected from their location within the cluster. Second, the proper motion is used to define the most probable members. Third, the selected members are plotted in a colour-magnitude diagram to derive age, distance, and reddening. Finally, this procedure is iterated until the best fit is achieved. The dispersion of the open circles in Figure 4.12 is mostly due to the error on the UCAC2 proper motion measurements (± 6 mas/yr), which is larger than the internal dispersion of the cluster. This dispersion indicates also that the sample of candidates is contaminated by field stars, as discussed previously. We have extracted 142 proper motion candidates (filled circles in Figure 4.12) within the circle defined above. Those objects are plotted as open triangles in the $(I, I-z)$ colour-magnitude diagram (Figure 4.6) and in the $(I-z, I-K)$ CCD (Figure 4.9).

The right panel of Figure 4.12 displays the $(I, I-z)$ colour-magnitude diagram for the optically-selected cluster member candidates in Collinder 359 with proper motion information from the Zacharias et al. (2003) catalogue. The best fit to the lower envelope of the cluster sequence (filled circles in Figure 4.12) is obtained for a distance of 500 pc and an age of 80 Myr (solid line in Figure 4.12). Other ages such as 30 Myr and 50 Myr appear too young for the cluster sequence as they tend to predict redder colours than those observed in the $I = 14-15$ magnitude range. Ages older than 80 Myr could also be possible, implying smaller distances. Note that the distance can be larger by about 50 pc if we take into account a mean extinction of 0.2 mag along the line of

sight of the cluster.

The sequence of proper motion candidates (filled circles in Figure 4.12) is about 0.1–0.2 mag wide. The reddest objects at bright magnitudes are likely field stars, effect not excluded due to the low galactic latitude of the cluster. We could also expect the presence of a binary sequence widening the cluster sequence.

The distance and age estimates from proper motion and photometry are certainly more reliable than turn-off main-sequence fitting technique based on a single high-mass star, 67 Oph. Furthermore, our estimate relies on a larger sample of cluster candidates than the former estimates from Van't-Veer (1980) and Ruciński (1987). Therefore, **we would favour a mean age of 80 Myr with an uncertainty of 20 Myr and distances of 500 ± 100 pc for Collinder 359.**

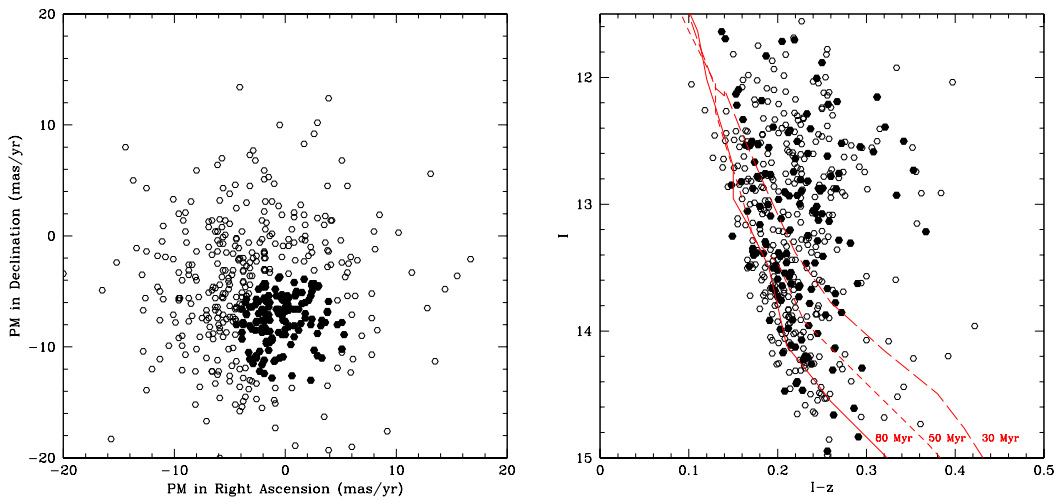


Figure 4.12: *Left panel:* Vector point diagram for optically-selected candidates common to the Zacharias et al. (2003) catalogue (open circles), including the ones with proper motion consistent with the cluster (filled circles). *Right panel:* ($I, I-z$) colour-magnitude diagram for the selected proper motion candidates. Filled and open circles have the same meaning as for the left panel. The solid, dashed, and long dashed lines correspond to the NextGen 80, 50, and 30 Myr isochrones, respectively (Baraffe et al. 1998). The lower envelope of the filled circles is best fit by a distance of 500 pc and an age of 80 Myr.

4.5.4 The cluster luminosity function

According to the results presented in the previous sections (§ 4.5.1–§ 4.5.3), we will assume a mean age of 80 Myr and a distance of 500 pc (distance modulus of 8.5 mag) for Collinder 359 to derive the cluster luminosity function (Figure 4.13 and Table 4.13). We remind that the uncertainty on the age and the distance of the cluster are 20 Myr and 100 pc, respectively. Nevertheless, we will address the issue regarding the influence of the age and the distance on the shape of the cluster luminosity function. We will consider here *only* the probable (Y+) cluster member candidates in

Collinder 359 from the results of the optical and the near-infrared photometry. We did not apply any selection based on proper motion measurements.

We have employed two approaches to derive the cluster luminosity function. The first approach consisted in counting the number of stars per bin of 0.5 mag (open squares in Figure 4.13). The second approach “smoothed” the luminosity function to better characterise the faint end, i.e. we have counted the number of stars per interval of 1.0 magnitude with steps of 0.5 magnitude (filled circles in Figure 4.13). Both methods yielded similar cluster luminosity functions.

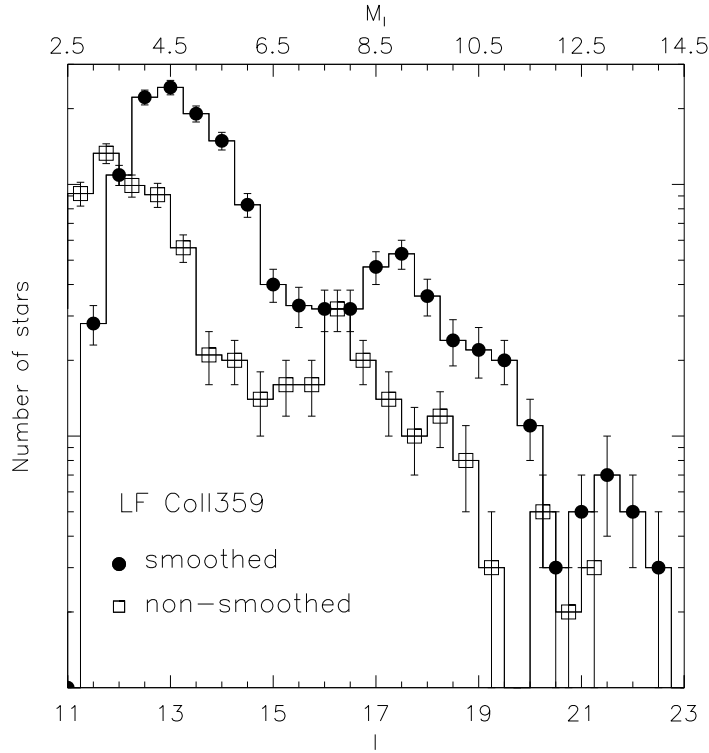


Figure 4.13: The cluster luminosity function assuming an age of 80 Myr and a distance of 500 pc for Collinder 359. The open squares represent the number of stars per bin of 0.5 magnitude whereas the filled circles indicate the number of stars in a 1.0 magnitude bin by step of 0.5 magnitudes. Poisson errors associated to the cluster luminosity function are indicated by vertical lines. Table 4.13 provides the number of stars per magnitude bin for the smoothed luminosity function.

Several features seen in the cluster luminosity function (Figure 4.13) are described below.

- A peak at $I = 12.5\text{--}13.0$ mag corresponding to approximately $1.0 M_{\odot}$ at an age of 80 Myr and a distance of 500 pc. The decline at brighter ($I \geq 12.5$) magnitudes reflects the incompleteness of the optical survey in that magnitude range caused by the saturation of the short exposures. The cross-correlation between the optically-selected cluster member candidates and the UCAC2 catalogue (Zacharias et al. 2003) indicates that a large number of objects have proper motions consistent with membership (Figure 4.12). However, the dispersion in the vector point diagram confirms a significant contamination by field stars difficult to

quantify at this stage.

- A peak at $I = 17.0\text{--}17.5$ mag ($M_I = 8.5\text{--}9.0$ mag) corresponding to masses of approximately $0.30 M_\odot$. A comparable peak is seen at $M_I = 11$ mag in NGC2516 (Jeffries et al. 2001), while this feature is detected at $M_I = 9$ mag in M35 (Barrado y Navascués et al. 2001) and $M_I = 10$ mag in α Per (Barrado y Navascués et al. 2002). This peak does not occur at the same absolute magnitude in all clusters, implying that it may be age dependent. This feature may correspond to the H₂-convection peak identified by Kroupa et al. (1990, 1993) in the luminosity function of nearby field stars but this hypothesis should be further investigated.
- A dip at $I = 20.0\text{--}20.5$ mag ($M \sim 0.070 M_\odot$) is clearly detected in the colour-magnitude diagram (Figure 4.6) well above our completeness limit. This feature is comparable to the gap seen in the α Per luminosity function at $M_I = 12.5$ mag (Barrado y Navascués et al. 2002). This dip is detected both in the field (Reid & Cruz 2002) and in young clusters, including σ Orionis (Béjar et al. 2001), the Trapezium Cluster (Lucas & Roche 2000), IC348 (Luhman 1999), the Pleiades (Jameson et al. 2002), and IC 2391 (Barrado y Navascués et al. 2001a). Despite the difference in age between the regions mentioned above, Jameson et al. (2002) argued that this gap is universal as it occurs consistently at the same spectral types. This feature might originate from the sharp fall in the luminosity-mass relation due to the formation of large dust grains at low temperatures around spectral types M7–M8 (Jameson et al. 2002). Considering the intrinsic colours versus spectral types given in Table 7 in Luhman et al. (2003b), a M7 dwarf has a $I-z = 0.98$ (no extinction is taken into account for this estimate). The observed dip in the colour-magnitude diagram for Collinder 359 occurs at $I-z = 0.85\text{--}1.00$ mag. However, IC348 is younger than Collinder 359, yielding hotter effective temperature at a given spectral type. Taking into account the uncertainties on the photometry (± 0.05 mag) and on the spectral type determination (half a subclass error), it is possible that the gap in the luminosity function is caused by the deficit of M7–M8 dwarfs.

4.6 The mass function of Collinder 359

4.6.1 The mass-magnitude relation

To transform the luminosity function of Collinder 359 into a mass function, we have used the NextGen and Dusty models from the Lyon group. For a given age and mass, the evolutionary models predict optical ($VRIz$) and near-infrared (JHK) absolute magnitudes. The I and z magnitudes were specifically computed for the CFH12K filters and we will use them to derive the mass function. We have merged both isochrone files to create a magnitude-mass relationship from 1.4 down to $0.010 M_\odot$. The NextGen isochrones are used for effective temperatures higher than 2500 K, corresponding to masses of $0.050 M_\odot$ at 80 Myr ($M_I \sim 13.0$ mag). These isochrones are completed by the Dusty models for lower masses down to $20 M_{Jup}$ ($M_I \sim 19.1$ mag at 80 Myr). The useful range of the merged isochrones in the course of our study of Collinder 359 is $1.3\text{--}0.030 M_\odot$.

The NextGen and Dusty models include the treatment of the atmospheres in contrast to other evolutionary models, such as those of D'Antona & Mazzitelli (1994), which assume grey atmospheres. These assumptions generally lead to higher effective temperatures and luminosities at a

Table 4.13: Number of stars per magnitude bin (luminosity function) and number of stars per mass bin in M_{\odot} (mass function) in Collinder 359, assuming a distance of 500 pc and an age of 80 Myr for the cluster. The luminosity function was transformed into a mass function using the NextGen and Dusty evolutionary models for masses higher and lower than $50 M_{Jup}$, respectively. The uncertainties quoted for the luminosity function are Poisson errors (square root of the number of stars per magnitude bin). The transformation of the luminosity function into a mass function was achieved by dividing the number of objects per magnitude bin by the difference of the upper and lower mass limit of the bin.

Mag bin	Mid-mass (M_{\odot})	Nb per mag bin	Nb per mass (M_{\odot})
11.0–12.0	1.390	28 ± 5	86 ± 15
11.5–12.5	1.241	109 ± 10	409 ± 37
12.0–13.0	1.124	222 ± 15	1002 ± 67
12.5–13.5	1.020	243 ± 16	1216 ± 80
13.0–14.0	0.924	191 ± 14	1073 ± 78
13.5–14.5	0.842	149 ± 12	876 ± 70
14.0–15.0	0.754	83 ± 9	468 ± 50
14.5–15.5	0.664	40 ± 6	277 ± 41
15.0–16.0	0.609	33 ± 6	283 ± 51
15.5–16.5	0.548	32 ± 6	233 ± 43
16.0–17.0	0.472	32 ± 6	190 ± 35
16.5–17.5	0.380	47 ± 7	256 ± 38
17.0–18.0	0.290	53 ± 7	326 ± 43
17.5–18.5	0.217	36 ± 6	291 ± 48
18.0–19.0	0.166	24 ± 5	272 ± 56
18.5–19.5	0.129	22 ± 5	348 ± 79
19.0–20.0	0.103	20 ± 4	439 ± 87
19.5–20.5	0.084	11 ± 3	328 ± 89
20.0–21.0	0.069	3 ± 2	120 ± 80
20.5–21.5	0.059	5 ± 2	210 ± 84
21.0–22.0	0.046	7 ± 3	378 ± 162
21.5–22.5	0.040	5 ± 2	574 ± 229
22.0–23.0	0.037	3 ± 2	446 ± 297

given mass. Furthermore, the treatment of the atmospheres predicts absolute magnitudes in various passbands, hence avoiding the use of bolometric corrections which remain highly uncertain for young open clusters. The models of Burrows et al. (2001) include non-gray atmospheres but are valid for masses lower than $0.1 M_{\odot}$, not low enough for our study. Finally, the Dusty models include the treatment of dust settling which affects the temperatures and observed colours of low-mass stars and brown dwarfs. The influence of the dust settling at the L/T transition around 1300 K for field objects has been proven and observed. The same effect will take place at earlier spectral types (late-M and early-L) in pre-main-sequence clusters due to the younger ages. The knowledge of opacity line lists for species such as TiO and VO, which are responsible for the shape of M dwarf spectra, is of prime importance to reproduce the observed colours of young cluster members.

Moreover, the evolutionary models from the Lyon group have been extensively used to estimate mass functions in open clusters, including the Pleiades (Martín et al. 1998; Dobbie et al. 2002;

Moraux et al. 2003), α Per (Barrado y Navascués et al. 2002), and M35 (Barrado y Navascués et al. 2001), and star-forming regions such as Taurus (Briceño et al. 2002) and IC348 (Luhman et al. 2003b). The NextGen and Dusty models have been the most successful evolutionary models in predicting coeval ages for the different components of the young multiple system GG Tau (White et al. 1999). Furthermore, different models from various groups had little effect on the mass function in α Per (Barrado y Navascués et al. 2002) and M35 (Barrado y Navascués et al. 2001). Finally, the mass estimates from evolutionary models appear generally underestimated by 5 to 20 % for main-sequence stars and by up to 50 % for pre-main-sequence stars (Hillenbrand & White 2004).

4.6.2 The cluster mass function

We have converted the cluster luminosity function into a mass function using the evolutionary models from the Lyon group (Baraffe et al. 1998; Chabrier et al. 2000b). The number of objects per unit of mass (dN/dM) is obtained by dividing the number of objects per magnitude bin (ΔN) by the difference between the upper and lower limits of the bin in mass ($\Delta M = M_2 - M_1$). The uncertainty is computed from the Poisson uncertainties of the luminosity function. For example, the magnitude range $I = 12\text{--}13$ mag corresponds to a mass range of $M = 1.241\text{--}1.020 M_{\odot}$. The number of objects per unit of mass and its uncertainty (Table 4.13) is given by:

$$\frac{dN}{dM} = \frac{\Delta N}{\Delta M} = \frac{222}{1.241 - 1.020} \pm \frac{\sqrt{222}}{1.241 - 1.020} = 1002 \pm 67$$

The mean mass and the number of stars per mass bin are given in Table 4.13. The mass function is plotted as filled circles in Figure 4.14. We will express the cluster mass function throughout this section as the mass spectrum (α represents the slope of the mass spectrum), namely:

$$\frac{dN}{dM} \propto M^{-\alpha}$$

The best linear fit to the cluster mass spectra, assuming an age of 80 Myr and a distance of 500 pc for Collinder 359, is obtained for $\alpha = 0.30$ (solid line in Figure 4.14).

Three major features are seen in the cluster mass function and described below:

- A peak at about $1 M_{\odot}$ which is not real due to the large field contamination observed in this range. Additional observations are needed to estimate the level of contamination in the $0.7\text{--}1.3 M_{\odot}$ mass range, at the distance and age of the cluster.
- A slow rise in the cluster mass function from $0.6 M_{\odot}$ down to our completeness limit at about $0.040 M_{\odot}$. The power law index α appears flatter than the Pleiades estimates.
- A dip in the mass function occurs around $0.070 M_{\odot}$ and is likely due to the dearth of M7–M8 objects. This gap is detected in the field (Reid & Cruz 2002) and in six open clusters, including the Pleiades (Jameson et al. 2002) and α Per (Barrado y Navascués et al. 2002). This argument is validated by the intrinsic colours of M7 dwarfs as defined by Luhman et al. (2003b) in the case of the IC348 cluster (see discussion in previous section).

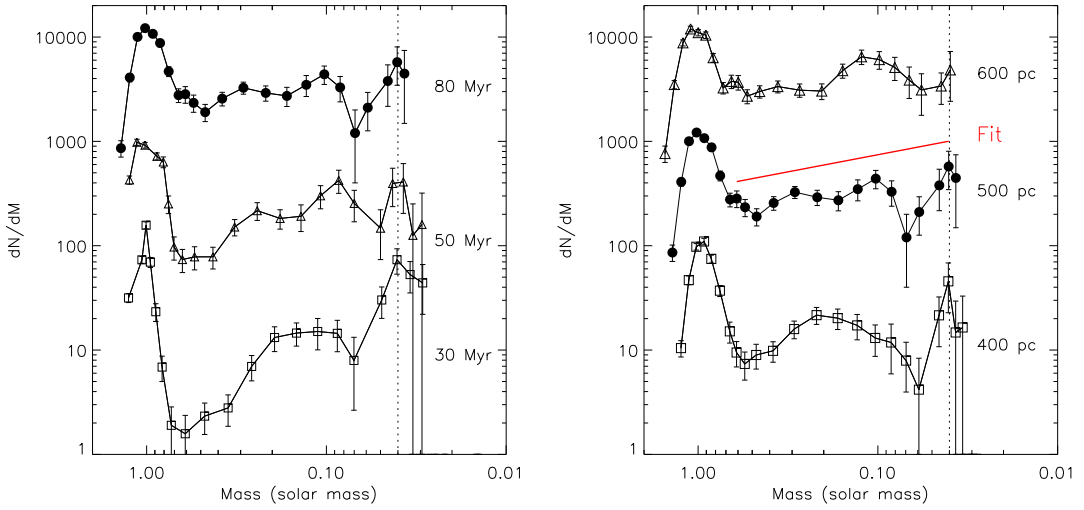


Figure 4.14: Mass function for Collinder 359. Filled circles represent the cluster mass function, assuming a distance of 500 pc and an age of 80 Myr for Collinder 359. *Left panel:* Influence of the age on the mass function for 30 Myr (open squares), 50 Myr (open triangles), and 80 Myr (filled circles). The slope of the mass function gets steeper for younger ages. *Right panel:* Influence of the distance on the mass function for 400 pc (open squares), 500 pc (filled circles), and 600 pc (open triangles), assuming an age of 80 Myr. The distance appears to have little influence on the slope of the mass function. The vertical dotted line represents the completeness of the CFH12K optical survey at $I = 22$, corresponding to a mass of $0.040 M_{\odot}$ at the assumed age and distance for the cluster. The three mass functions are offset for clarity.

Table 4.14: Dependence of the power law index α with distance and age in Collinder 359. We have used linear fits to estimate the slope of the mass spectrum, assuming different (distance, age) combinations for the cluster. The three ages are 30, 50, and 80 Myr assuming a distance of 500 pc. The three distances are 400, 500, and 600 pc, assuming a mean age of 80 Myr.

Age	Distance	Mass range	Power law index
80 Myr	400 pc	$M = 0.55 - 0.035 M_{\odot}$	$\alpha = 0.35 \pm 0.15$
	500 pc	$M = 0.61 - 0.040 M_{\odot}$	$\alpha = 0.30 \pm 0.10$
	600 pc	$M = 0.65 - 0.044 M_{\odot}$	$\alpha = 0.25 \pm 0.10$
50 Myr	400 pc	$M = 0.43 - 0.030 M_{\odot}$	$\alpha = 0.60 \pm 0.15$
	500 pc	$M = 0.54 - 0.030 M_{\odot}$	$\alpha = 0.45 \pm 0.10$
	600 pc	$M = 0.62 - 0.032 M_{\odot}$	$\alpha = 0.45 \pm 0.10$
30 Myr	400 pc	$M = 0.60 - 0.030 M_{\odot}$	$\alpha = 1.0 \pm 0.2$
	500 pc	$M = 0.70 - 0.030 M_{\odot}$	$\alpha = 1.0 \pm 0.2$
	600 pc	$M = 0.58 - 0.030 M_{\odot}$	$\alpha = 0.5 \pm 0.1$

We have investigated the influence of the age and the distance on the cluster mass spectrum. In the left panel in Figure 4.14, we have plotted the mass spectrum in Collinder 359 for three ages,

including 30 Myr (open squares), 50 Myr (open triangles), and 80 Myr (filled circles), assuming a distance of 500 pc. In the right panel in Figure 4.14, we have plotted the mass spectrum for three distances, including 400 pc (open squares), 500 pc (filled circles), and 600 pc (open triangles), assuming an age of 80 Myr.

We have used linear fits to estimate the slopes for each (distance, age) combination (Table 4.14). The change in distance (± 100 pc) seems to have little influence on the power law index α , independent of the assumed age. On the contrary, the slope of the mass spectrum tends to increase with younger ages, ranging from $\alpha = 0.3$ at 80 Myr to $\alpha = 1.0$ at 30 Myr. The gap observed around $0.070 M_{\odot}$ persists independent of the (distance, age) combination, implying that it is likely a real feature.

As the age of Collinder 359 is likely between 60 and 100 Myr and the distance 500 ± 100 pc, we conclude that the best fit to the cluster mass spectrum is obtained for a power law index $\alpha = 0.30 \pm 0.20$ over the mass range $0.60\text{--}0.04 M_{\odot}$.

4.6.3 Uncertainties on the cluster mass function

The derivation of the cluster mass function is, in theory, a straightforward process. Based on the selected cluster members, we count the number of stars per magnitude bins to create a luminosity function. To transform the luminosity function into a mass function, we apply a magnitude-mass relationship provided by evolutionary models. For a given age and a given mass, the evolutionary models provide luminosities and effective temperatures. However, in practice, the cluster mass function determination is hampered by multiple factors sometimes difficult to quantify.

1. The largest uncertainty resides in the distance of Collinder 359. Larger and smaller distances will shift objects towards higher and lower masses, respectively. We have assumed a distance of 500 pc for Collinder 359 and shown that distances spanning 400–600 pc have little influence on the overall shape of the mass function.
2. The second uncertainty concerns the age of Collinder 359. Older and younger ages will shift the objects towards higher and lower masses, respectively, with a tendency to increase the slope of the mass spectrum at younger ages.
3. Some objects might have escaped detection within the 1.6 square degree area surveyed in Collinder 359. Despite the good cosmetics of the CFH12K camera, some bona-fide cluster members might lie on a bad column or have their photometry affected by bad pixels. Similarly, bright stars hamper the detection of nearby faint cluster members. This effect is likely to be random. If the bias is larger towards fainter objects, α may have to be increased. Our ability of detecting substellar objects is affected by the fact that the luminosity of brown dwarfs decreases with age (de la Fuente Marcos & de la Fuente Marcos 2000).
4. A large number of faint ($I \geq 17$ mag) cluster member candidates are still lacking near-infrared photometry. Furthermore, optical spectroscopy is required to ascertain the membership of the selected candidates. As an example, the contamination was estimated at $\sim 25\text{--}40\%$ for low-mass stars and brown dwarfs in the Pleiades (Bouvier et al. 1998; Martín et al. 2000a; Moraux et al. 2001), and in α Per (Barrado y Navascués et al. 2002). We expect a comparable level of contamination in Collinder 359 due to its intermediate galactic latitude. If the contamination is larger in the brown dwarf regime than for low-mass stars, α may have to be decreased.

5. According to estimates from Kharchenko et al. (2004, personal communication), we have mainly focused on the cluster corona. If Collinder 359 is indeed a cluster younger than the Pleiades, the mass segregation and evaporation of brown dwarfs should be less than 10 %, assuming an homogeneous distribution of substellar objects across the cluster (de la Fuente Marcos & de la Fuente Marcos 2000). In contrast, if the cluster is older than the estimates presented here and if dynamical evolution has already taken place, the number of very low-mass stars and brown dwarfs detected in the surveyed area has been well overestimated. The α index may have to be increased according to the amount of brown dwarfs which have escaped the cluster.
6. We have used the magnitude-mass relationship from the Lyon group and combined the NextGen and Dusty models to infer a mass function from 1.3 to $0.040 M_{\odot}$. Other evolutionary models assume grey atmospheres (e.g. D'Antona & Mazzitelli 1994) and tend to predict higher effective temperatures and luminosities so α would have to be decreased. However, Barrado y Navascués et al. (2001, 2002) have shown that various evolutionary models had little influence on the α Per and M35 mass functions. A thorough comparison of a large sample of stars with different evolutionary tracks by Hillenbrand & White (2004) indicates that masses of main-sequence and pre-main-sequence objects are underestimated. The effect on the shape of the mass spectrum is difficult to assess in that case.
7. We have neglected the effect of unresolved binaries. For example, a brown dwarf in the Pleiades, PPI15 (Rebolo et al. 1995) was resolved into a spectroscopic binary brown dwarf (Basri & Martín 1999a). The influence of unresolved binaries in open clusters was quantified by Kroupa (2001), implying that the power law index α should be increased by about 0.5 over the $1.0-0.1 M_{\odot}$ mass range. Martín et al. (2000a) failed to detect companions in Pleiades brown dwarf candidates with separations wider than 27 AU at the distance of the cluster, suggesting that the binary frequency of brown dwarfs is not much larger than for M dwarfs and has little effect on the shape of the mass function. If the binary correction is important at low masses (for example if a large number of M dwarfs are binaries), α may have to be increased.
8. A possible age spread in the cluster was not considered throughout this study. Spectroscopic confirmation is required to place the cluster members in the HR diagram in order to estimate this effect.

To summarise, large uncertainties remain regarding the mass function in Collinder 359 which led us to consider a conservative error on the slope of the cluster mass function i.e. $\alpha = 0.3 \pm 0.2$ over the $0.6-0.04 M_{\odot}$ mass range.

4.6.4 Comparison with other young clusters

We have compared the mass function for Collinder 359 with estimates available in the literature for other young open clusters and star-forming regions. Figure 4.15 compares the mass function for Collinder 359 (filled circles) with α Per (Barrado y Navascués et al. 2002), M35 (Barrado y Navascués et al. 2001), and various estimates of the Pleiades mass spectrum (Bouvier et al. 1998; Martín et al. 1998; Dobbie et al. 2002; Tej et al. 2002).

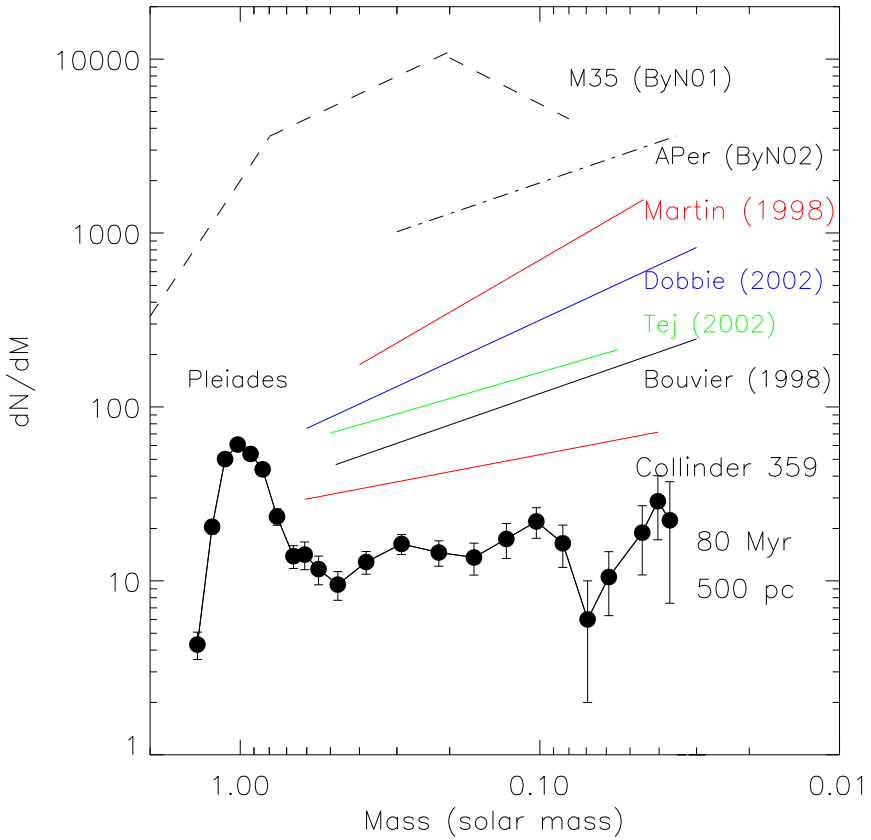


Figure 4.15: Comparison of the mas spectrum for Collinder 359 (filled circles with solid line) with other open clusters, including α Per (dot-dashed line; Barrado y Navascués et al. 2002), M35 (dashed line; Barrado y Navascués et al. 2001), and the Pleiades (Martín et al. 1998; Bouvier et al. 1998; Dobbie et al. 2002; Tej et al. 2002). The best linear fit to the cluster mass spectrum (red line) appears flatter than the Pleiades over the $0.55\text{--}0.035 M_\odot$ mass range. The peak at $\sim 1 M_\odot$ is not a real feature but the outcome of a large contamination at higher masses.

Across the stellar/substellar boundary, the power law indices estimated in the Pleiades by various groups were generally in good agreement within the errors with $\alpha=0.5\text{--}1.0$ in the $0.40\text{--}0.045 M_\odot$ mass range (Figure 4.15; Table 1.1 in Chapter 1).

Barrado y Navascués et al. (2002) has inferred a comparable mass function for the α Per cluster with $\alpha=0.59\pm0.05$ from 0.30 to $0.035 M_\odot$ (Figure 4.15; Chapter 3).

Concerning M35, the mass spectrum was approximated by a three-segment power law over the $6\text{--}0.08 M_\odot$ mass range (Figure 4.15; Barrado y Navascués et al. 2001).

The mass spectrum derived for Collinder 359 is overall consistent within the uncertainties with various estimates in open cluster and star-forming regions. Our result appear however flatter than the Pleiades and α Per estimates (Figure 4.15) although they might be considered in agreement within the error bars (0.1 and 0.2 for the Pleiades and Collinder 359, respectively).

Compared to other well-studied regions mentioned above, our estimate is solely based on optical and near-infrared photometric selection. The next step is to obtain low-resolution spectroscopy for all selected cluster member candidates in Collinder 359 to verify the validity of the mass function and the various observed dips and gaps. If confirmed, the gap at $0.070 M_{\odot}$ combined with the search for the lithium depletion boundary would add strong constraints on the age and the distance of the cluster and confirm the present estimates.

4.7 Conclusions of the survey in Collinder 359 and perspectives

We have presented in this chapter the first deep optical wide-field imaging survey complemented with near-infrared follow-up observations of the young open cluster Collinder 359. We have surveyed 1.6 square degrees in the cluster in the I and z filters down to detection and completeness limits of 22.0 and 24.0 with the CFH12K on the Canada-France-Hawaii 3.6-m telescope. Based on their location in the optical ($I, I-z$) colour-magnitude diagram, we have extracted a total of 1033 cluster member candidates in Collinder 359 spanning $1.3-0.040 M_{\odot}$, assuming a distance of 650 pc and an age of 80 Myr. We have cross-correlated the optically-selected candidates with the 2MASS database for objects brighter than $I = 17.0$ to weed out contaminating field stars. Further K' -band photometry has been obtained for a subsample of 39 faint cluster candidates to probe the contamination at and below the stellar/substellar boundary.

By comparing the location of the brightest cluster member, 67 Oph, with solar metallicity isochrones including moderate overshoot, we have derived an age of 60 ± 20 Myr for Collinder 359. The comparison of the NextGen evolutionary models to the cluster candidates selected from their proper motion and colours yielded a mean age of 80 Myr with an uncertainty of 20 Myr and a distance of 500 ± 100 pc. The age is larger than previous estimates in the literature, whereas the distance is within the uncertainties of former determinations but based on a larger number of objects. Hence, Collinder 359 is probably not a pre-main-sequence cluster (10–50 Myr) as thought earlier but likely coeval with α Per. The question set in § 4.1 regarding the test of pre-main-sequence evolutionary tracks with clusters 10–50 Myr old might not be solved with the study of Collinder 359.

Finally, we have derived luminosity and mass functions for Collinder 359 using the NextGen and Dusty models from the Lyon group. Despite the uncertainties inherent to photometric surveys in open clusters, we have reported a dip in the luminosity and mass functions located at $I = 20.5$ (corresponding to a mass of $70 M_{Jup}$) assuming a mean age of 80 Myr and a distance of 500 pc) likely caused by the dearth of M7–M8 dwarfs observed in the solar neighbourhood and young clusters. The best fit to the slope of the mass function, when expressed as the mass spectrum is $\alpha = 0.30 \pm 0.20$ over the $0.55-0.035 M_{\odot}$ mass range. The derived slope is flatter than estimates in the Pleiades and in the α Per clusters although they are consistent within the uncertainties. Spectroscopy is needed to verify the results presented in this chapter as our work is solely based on photometry. Our study do not provide a convincing evidence for a variable mass spectrum in open clusters.

The detailed study of Collinder 359 constitutes a first step towards the determination of an unbiased mass function in a previously unstudied young open cluster. Follow-up observations of the selected cluster member candidates in Collinder 359 are required to ascertain their membership,

including near-infrared imaging and optical spectroscopy. We have been granted observing time with several telescopes and instruments within the framework of the CFHT Key Programme to pursue our investigation of Collinder 359 and other pre-main-sequence clusters. The time schedule and the observations are divided as follows:

CFHT/CFHTIR	4 nights (30 May–03 June 2004)	Near-infrared imaging
Calar Alto 2.2-m/MAGIC	4 nights (10–13 June 2004)	Near-infrared imaging
WHT/AF2/WYFFOS	6 nights (18–24 June 2004)	Multi-object spectroscopy
TNG/DOLORES	3 nights (19–21 June 2004)	Optical spectroscopy

Near-infrared imaging will be obtained for the remaining faint ($I \geq 17.0$) cluster member candidates in Collinder 359 to probe the contamination by field stars at and below the hydrogen-burning limit. Low-resolution ($R \sim 600$) optical (6000–10000 Å) spectroscopy will provide spectral classification, gravity measurements, and determination of the level of chromospheric activity, which, together, will allow us to further constrain the membership of cluster candidates.

Longer term observations are foreseen to enlarge our study of Collinder 359. For example, higher resolution optical spectroscopy of the bright cluster members will provide radial and rotational velocities to study the dependence of these parameters with mass and age. Additionally, the inner square degree area in Collinder 359 remains to be surveyed to confirm the results presented in this chapter. Finally, objects brighter than $I \sim 12.0$ and thus more massive than $\sim 1 M_{\odot}$ should be investigated to derive a complete mass function from higher mass stars down to brown dwarfs.